REFERENCE MULTIGROUP CROSS SECTION RESULTS OF STYLIZED MICROREACTOR BENCHMARK PROBLEMS

A Thesis
Presented to
The Academic Faculty

by

Aaron Sommer

In Partial Fulfillment
of the Requirements for the Degree
Master of Science in Nuclear Engineering in the
George W. Woodruff School of Mechanical Engineering

Georgia Institute of Technology
December 2022

REFERENCE MULTIGROUP CROSS SECTION RESULTS OF STYLIZED MICROREACTOR BENCHMARK PROBLEMS

Approved by:

Dr. Farzad Rahnema, Advisor
George W. Woodruff School
Georgia Institute of Technology

Dr. Dingkang Zhang
George W. Woodruff School
Georgia Institute of Technology

Dr. Abderrafi Ougouag
Idaho National Laboratory

Date Approved: November 30, 2022

ACKNOWLEDGEMENTS

I would like to express my gratitude to my advisor, Dr. Farzad Rahnema, as well as Dr. Dingkang Zhang and Dr. Abderrafi Ougouag for serving on my thesis committee as well as their advice and feedback on this work. This experience serves as the first step to the rest of my career in graduate studies and beyond, and this would not be possible without their guidance on presenting this work with the thoroughness and importance it deserves. I applaud them for remaining faithful in and guiding this work throughout a master's program derailed early on by the pandemic, and at last have something to bear fruit.

I also would like to thank the Department of Energy's Office of Nuclear Energy, as this research was funded under the Nuclear Energy University Program Graduate Fellowship. The contents in this work made use of Idaho National Laboratory computing resources also supported by the Office of Nuclear Energy, as well as the Nuclear Science User Facilities under Contract No. DE-AC07-05ID14517.

TABLE OF CONTENTS

ACKNOWLEDGEMENTS **iii**

LIST OF TABLES **vi**

LIST OF FIGURES **ix**

LIST OF SYMBOLS AND ABBREVIATIONS **x**

SUMMARY **xii**

CHAPTER 1. Introduction **1**

CHAPTER 2. Core Specification **4**
2.1 Radial Layout **4**
2.2 Axial Layout **5**
2.3 Assembly Geometric Specifications **6**
2.3.1 Fuel Assembly 6
2.3.2 Control Drum Assembly 8
2.3.3 Reflector Block 9
2.4 Temperature Specifications **10**
2.5 Isotopic Compositions **12**

CHAPTER 3. Methodology **14**

CHAPTER 4. Results and Conclusions **22**
4.1 Reference Solutions **23**
4.1.1 Eigenvalues 23
4.1.2 Fission Rate Distributions 24
4.1.3 Flux Spectra 28
4.2 Two-Group Macroscopic Data for 2D Single Assembly **31**
4.2.1 Fast Data 32
4.2.2 Thermal Data 34
4.2.3 Discussion 35
4.3 Four-Group Scattering Kernels for 2D Single Assembly **37**
4.3.1 Legendre Moments 38
4.3.2 Discussion 40
4.4 Selected Two-Group Macroscopic Data in Core Configurations **40**
4.4.1 Beryllium Fast Macroscopic Scattering Cross Sections 41
4.4.2 EuB_6 Thermal Macroscopic Absorption Cross Sections 41
4.4.3 Discussion 42
4.5 Comparison of Core Configuration Data against 2D Single Assembly Data **43**
4.5.1 Macroscopic Capture Cross Sections 44
4.5.2 Macroscopic Scattering Cross Sections 47
4.5.3 Macroscopic Fission Cross Sections 53
4.5.4 Discussion 55

4.6 Comparison of 3D Single Assembly Data against 2D Single Assembly Data 55
4.6.1 Macroscopic Capture Cross Sections 57
4.6.2 Macroscopic Scattering Cross Sections 58
4.6.3 Macroscopic Fission Cross Sections 61
4.6.4 Macroscopic Nubars 62
4.6.5 Discussion 63

CHAPTER 5. Future Work 64

APPENDIX A. Summary of Attached Files 65
A.1 Multigroup Cross Section and Nubar Files 65
A.1.1 File Naming Format 65
A.1.2 Input File Structure 66
A.1.3 Main Output File Structure 67
A.1.4 Detector Output File Structure 68
A.2 Multigroup Scattering Kernel Files 69
A.3. Multigroup Data Tables 69

APPENDIX B. Example SERPENT 2 Input File 70

APPENDIX C. Selected Microscopic Cross Sections 76
C.1 Fast Data 76
C.2 Thermal Data 78

REFERENCES 79

LIST OF TABLES

Table 1 – Core Geometric Specifications1 4

Table 2 – Fuel Assembly Geometric Specifications1 8

Table 3 – Control Drum Assembly Geometric Specifications1 9

Table 4 – Uniform Material Temperatures 10

Table 5 – Atomic Density Data for Fuel, Moderator, Reflector, and Absorber1 12

Table 6 – Atomic Density Data for Heat Pipe and Monolith1 13

Table 7 – Upper Bounds of Multigroup Energy Structures 15

Table 8 – Computational Cost (CPU · hour) of Runs Performed 16

Table 9 – Benchmark Problem Eigenvalues 24

Table 10 – Normalized Pin Fission Distributions for Assembly Configurations 25

Table 11 – Normalized Pin Fission Distribution for Drums-in Core Configuration 26

Table 12 – Normalized Pin Fission Distribution for Drums-out Core Configuration 27

Table 13 – Macroscopic Data for Fuel Rods in 2D Assembly Configuration, Group 1 of 2 32

Table 14 – Macroscopic Data for Moderator Rods in 2D Assembly Configuration, Group 1 of 2 33

Table 15 – Macroscopic Data for Heat Pipes in 2D Assembly Configuration, Group 1 of 2 33

Table 16 – Macroscopic Data for Fuel Rods in 2D Assembly Configuration, Group 2 of 2 34

Table 17 – Macroscopic Data for Moderator Rods in 2D Assembly Configuration, Group 2 of 2 34

Table 18 – Macroscopic Data for Heat Pipes in 2D Assembly Configuration, Group 2 of 2 35

Table 19 – Four-Group P_0 Macroscopic Scattering Kernel Averaged Over 2D Assembly Configuration 38

Table 20 – Four-Group P_1 Macroscopic Scattering Kernel Averaged Over 2D Assembly Configuration 38

Table 21 – Four-Group P_2 Macroscopic Scattering Kernel Averaged Over 2D Assembly Configuration 39

Table 22 – Four-Group P_3 Macroscopic Scattering Kernel Averaged Over 2D Assembly Configuration 39

Table 23 – Macroscopic Scattering Cross Sections for Beryllium in Core Configurations, Group 1 of 2 41

Table 24 – Macroscopic Capture Cross Sections for EuB_6 in Core Configurations, Group 2 of 2 41

Table 25 – Error of Macroscopic Capture Cross Sections in Fuel Incurred by Using 2D Data to Approximate Drums-in Core Configuration, Group 2 of 8 44

Table 26 – Error of Macroscopic Capture Cross Sections in Fuel Incurred by Using 2D Data to Approximate Drums-out Core Configuration, Group 2 of 8 46

Table 27 – Error of Macroscopic Scattering Cross Sections in Fuel Incurred by Using 2D Data to Approximate Drums-in Core Configuration, Group 2 of 8 47

Table 28 – Error of Macroscopic Scattering Cross Sections in Fuel Incurred by Using 2D Data to Approximate Drums-out Core Configuration, Group 2 of 8 48

Table 29 – Error of Macroscopic Scattering Cross Sections in Moderator Incurred by Using 2D Data to Approximate Drums-in Core Configuration, Group 2 of 8 49

Table 30 – Error of Macroscopic Scattering Cross Sections in Moderator Incurred by Using 2D Data to Approximate Drums-out Core Configuration, Group 2 of 8 50

Table 31 – Error of Macroscopic Scattering Cross Sections in Heat Pipe Incurred by Using 2D Data to Approximate Drums-in Core Configuration, Group 2 of 8 51

Table 32 – Error of Macroscopic Scattering Cross Sections in Heat Pipe Incurred by Using 2D Data to Approximate Drums-out Core Configuration, Group 2 of 8 52

Table 33 – Error of Macroscopic Fission Cross Sections in Fuel Incurred by Using 2D Data to Approximate Drums-in Core Configuration, Group 2 of 8 53

Table 34 – Error of Macroscopic Fission Cross Sections in Fuel Incurred by Using 2D Data to Approximate Drums-out Core Configuration, Group 2 of 8 54

Table 35 – Error of Macroscopic Capture Cross Sections in Fuel Incurred by Using 2D Data to Approximate 3D Assembly Configurations, Group 2 of 8 57

Table 36 – Error of Macroscopic Scattering Cross Sections in Fuel Incurred by Using 2D Data to Approximate 3D Assembly Configurations, Group 2 of 8 58

Table 37 – Error of Macroscopic Scattering Cross Sections in Moderator Incurred by Using 2D Data to Approximate 3D Assembly Configurations, Group 2 of 8 59

Table 38 – Error of Macroscopic Scattering Cross Sections in Heat Pipe Incurred by Using 2D Data to Approximate 3D Assembly Configurations, Group 2 of 8 60

Table 39 – Error of Macroscopic Fission Cross Sections in Fuel Incurred by Using 2D Data to Approximate 3D Assembly Configurations, Group 2 of 8 61

Table 40 – Error of Macroscopic Nubars in Fuel Incurred by Using 2D Data to Approximate 3D Assembly Configurations, Group 2 of 8 62

Table 41 – Microscopic Data for Fuel in 2D Assembly Configuration, Group 1 of 2 76

Table 42 – Microscopic Data for Moderator in 2D Assembly Configuration, Group 1 of 2 77

Table 43 – Microscopic Data for Fuel in 2D Assembly Configuration, Group 2 of 2 78

Table 44 – Microscopic Data for Moderator in 2D Assembly Configuration, Group 2 of 2 78

LIST OF FIGURES

Figure 1 – XY View of Core with Control Drums Rotated Outward1 5

Figure 2 – XZ View of Core1 6

Figure 3 – XY View of Fuel Assembly1 7

Figure 4 – YZ View of Fuel Assembly1 7

Figure 5 – XY View of Control Drum1 9

Figure 6 – XY View of Assembly Slice with Pin Numbering 17

Figure 7 – XY View of Core Slice with Assembly Designation 18

Figure 8 – Normalized Fuel Flux Spectrum for Selected Assembly Configurations 28

Figure 9 – Normalized Moderator Flux Spectrum for Selected Assembly Configurations 29

Figure 10 – Normalized Fuel Flux Spectrum in Assembly B for Core Configurations 30

Figure 11 – Normalized Moderator Flux Spectrum in Assembly B for Core Configurations 31

Figure 12 – Infinite Assembly Lattice with Pin Numbering 36

LIST OF SYMBOLS AND ABBREVIATIONS

1σ	Statistical uncertainty, read "one-sigma"
2D	Two-dimensional, referring to an infinitely tall fuel assembly
3D	Three-dimensional, referring to a finitely tall fuel assembly
b	Barn, unit of microscopic cross section, equivalent to 10^{-24} cm^2
Be	Beryllium
E_g	Energy group/bin
EuB_6	Europium boride
eV	Electronvolt, unit of incident neutron energy
HP	Heat pipe
INL	Idaho National Laboratory
k_{eff}	Reactor criticality eigenvalue, read "k-effective"
keV	Kiloelectronvolt, equivalent to 10^3 eV
LANL	Los Alamos National Laboratory
meV	Millielectronvolt, equivalent to 10^{-3} eV
MeV	Megaelectronvolt, equivalent to 10^6 eV
(n, *n)	Production of multiple neutrons from incident neutron
Na	Sodium
$\bar{\nu}$	Nubar
pcm	*Per cent mille*, equivalent to 10^{-5}
PEI	Percent error incurred
φ	Neutron flux, scalar
ρ	Mass density, units of grams per cubic centimeter

RR	Reaction rate
Σ	Macroscopic cross section, units of one per centimeter
σ	Microscopic cross section, units of barn
Σ_{2D}	Macroscopic cross section in 2D assembly case
$\Sigma_{s,g'\rightarrow g}$	Macroscopic scattering cross section from energy group g' to g
SS316	Stainless steel alloy 316
UN	Uranium mononitride
V	Subregion volume
WEC	Westinghouse Electric Company
YH_2	Yttrium dihydride

SUMMARY

This thesis provides reference solutions and multigroup data of a series of neutronic benchmark problems based on the Empire design[1] developed by Los Alamos National Laboratory (LANL) for the Westinghouse Electric Company (WEC) eVinci microreactor concept[2]. The core design consists of eighteen identical fuel assemblies that each contain uranium mononitride (UN) as fuel and yttrium dihydride (YH_2) as moderator, and transfer heat outside the core via a series of heat pipes (HP). An outer layer composed of beryllium (Be) blocks, within some of which are rotatable control drums each containing a strip of europium boride (EuB_6) absorber, radially surrounds the core to provide a controllable amount of neutron reflection back into the core. The set of benchmark problems contains stylizations for simplicity in modeling in continuous energy Monte Carlo codes while retaining reactor physics features such as high core heterogeneity and leakage that are characteristic of the design.

In this thesis, the Empire design is first detailed below with geometric dimensions, isotopic fractions, and material densities as originally specified in the Idaho National Laboratory (INL) report[1], and average temperatures for some materials specified in a thermal hydraulic analysis of this design[3]. The gap in literature involving the average temperature for the beryllium reflectors and EuB6 absorber is addressed.

From this benchmark problem specification, six problem sets utilizing different core environmental effects are considered. The first problem set is a reference set consisting of a two-dimensional (2D) representation of a single fuel assembly generated by removing axial reflectors from the assembly and modeling the resulting geometry under

the specular reflective boundary condition so that an infinitely tall and axially uniform fuel assembly is simulated. Three problem sets involve a three-dimensional (3D) fuel assembly of finite height capped by axial reflectors under the following boundary conditions: vacuum, specular, and a mixed boundary condition where neutrons reflect radially and leak axially. involve a full core configuration of the Empire model with control drums rotated fully inward or outward to result in criticality extrema; both core configurations operate under the vacuum boundary condition. These problem sets are chosen to generate a wide variety of core environmental profiles.

The descriptions of the core model, the composing fuel assemblies, and problem set configurations are sufficient to create neutronic benchmark problems in an arbitrary transport code. Provided in this thesis are continuous energy Monte Carlo code SERPENT 2[4] reference solutions for each problem set of its eigenvalue (k_{eff}), flux spectrum averaged in fuel and moderator for each contained assembly, and radial and axial fission rate density distributions. Each problem set also has evaluated multigroup data for one-fifth axial divisions of selected pins in macroscopic and microscopic cross sections (XS) for total reaction, radiative capture, scattering, and fission and (n,2n) reaction if applicable to that division and energy group. In addition, up to third-order assembly-averaged multigroup Legendre moments of the scattering kernel are included. Electronic attachments to this thesis include all SERPENT 2 input files for each problem sets and their respective outputs, along with complete sets of multigroup data in tables formatted for readability like those found in the text. The attachments contain reference solutions and respective multigroup data and relative statistical uncertainties thereof for all problem sets, including those in the thesis text selected to highlight trends discovered in modeling the benchmark problem.

CHAPTER 1. INTRODUCTION

Nuclear microreactors have material and geometric characteristics that differ from traditional light water reactors. Microreactor designs, such as the Empire model studied in this thesis, contain control material and mechanisms near the core periphery and away from fissionable material, which results in a highly heterogenous material profile at both the single assembly and full core scales. The smaller dimensions employed by microreactor designs allows for a greater probability of neutron leakage. Evaluation of any core design at a given scenario is performed via utilizing precomputed multigroup cross sections in two-stage lattice diffusion or transport core calculation codes. The presence of core heterogeneity and neutron leakage influences the accurate generation of these cross sections and complicates the generation of such useful data in a reasonable amount of time.

Short term control of light water reactors is performed by mechanisms depending on their designs – via control rods inside a fuel assembly or neutron poison in the water between assemblies for pressurized water reactors, and inter-assembly control blades for boiling water reactors. The location of these control materials can be summarized across designs as inside or near a fuel assembly. The industry-standard two-step lattice transport codes exploit these placements. The first step is to model all fuel assemblies containing unique loadings with and without potential control material or reflectors to generate a library of multigroup cross section data detailing 2D assemblies of infinite axial height. The large size of the core and number of total assemblies allow for both the assumption of negligible core environment events as a function of assembly location as well as the use of the specular reflective boundary condition at the periphery of the fueled portion of the assembly to well approximate the flux spectra at the 3D assembly periphery. The second step is to use the data within the generated cross section libraries to model the whole core via transport theory or diffusion tools.

Heterogeneity in assembly and core configurations create core environmental effects that decrease the accuracy of the specular reflective boundary condition in approximating the true flux spectrum at the edges of a modeled assembly. To counteract this loss of accuracy, two-step methods can correct multigroup cross section data generated by the first step before input for core calculation in the second step[5]. However, the effect of these corrective measures diminishes with further heterogeneity and leakage, especially in microreactor designs with greatly segregated control and fissionable materials.

This thesis analyzes the Empire model due to the availability of literature in geometric specifications, material choices, isotopic compositions[1], and most material temperatures[3], and the expectation of a strong dependence of multigroup data on parameters like assembly location and interface boundary conditions based on the high heterogeneity and small dimensions of the design. Gaps in remaining material temperatures are filled to create a stylized model of the core. Further stylizations include the omission of support structures and thermal gradients and are performed to simplify the description of the model with a negligible effect on neutronics. The stylized model preserves core heterogeneity with minimized complexity.

Benchmark problems are generated from the unambiguous design definition with the addition of enforced boundary conditions on single fuel assemblies or configurations of multiple assemblies and control drums into core configurations. These problems have their respective solutions and multigroup data evaluated using SERPENT 2[4] and presented in this thesis either in text or in attached electronic data. The rationale for the publication of the above data is to provide accurate references for benchmarking reactor physics computation methods.

CHAPTER 2. CORE SPECIFICATION

The INL report[1] contains the full geometric specification of the design and isotopic compositions of the materials used within. This design utilizes a core loading of 2,352.1 kg of UN at 19.75% atomic enrichment. Table 1 details the basic geometric specifications of the core and the comprising lattice of assemblies.

Table 1 – Core Geometric Specifications[1]

Parameter	Value
Assembly apothem	16.0765 cm
Assembly triangular pitch	32.553 cm
Inter-block gap	0.4 cm
Active core height	60 cm
Core apothem	97.659 cm

2.1 Radial Layout

Figure 1 depicts a two-dimensional, 280 × 280 cm view of a core configuration built in a hexagonal shape and containing a hexagonal assembly lattice. The center of this lattice is empty to allow room for shutdown control mechanisms and is therefore modeled as void. Surrounding this central region are assemblies containing fuel, absorber, or pure beryllium. The inner two rings are composed of respectively, six and twelve identical fuel assemblies shaped as regular hexagons of apothem 16.0765 cm. Outside these fuel assemblies are six control mechanisms each composed of a circular strip of EuB_6 (red in Figure 1) absorber embedded with a beryllium (green in Figure 1) drum surrounded by beryllium filling a hexagon of the same dimensions as the fuel assembly. All remaining spaces are pure beryllium blocks of whatever part of the assembly shape allowed by the core periphery.

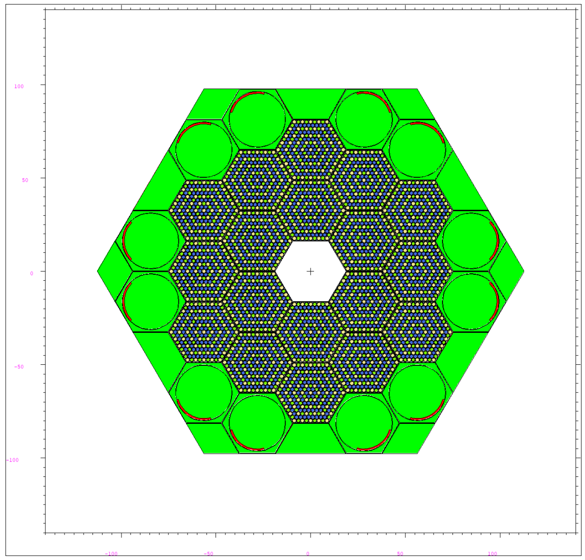

Figure 1 – XY View of Core with Control Drums Rotated Outward[1]

The rotation of these control drums is the method of changing the criticality of the core. Figure 1 shows the configuration that maximizes k_{eff} when the drums are rotated outward, moving reflector closer to and neutron poison farther away from the core radial center. Its counterpart is the fully controlled configuration that moves the poison in front of the drum body via rotating the drums fully inward. Henceforth these two configurations will be respectively written as “drums-out” and “drums-in” and represent the extrema in eigenvalue allowable by the construction of the core.

2.2 Axial Layout

All assemblies are axially uniform, each having height of 60 cm and being flush with one another. Fuel assemblies are capped on top and bottom by axial beryllium reflectors. Figure 2 depicts a 280 × 280 cm axial view centered near the center of the core. The model described in thesis does not account for holes to allow heat pipes to transfer power outside of the core; this stylization is performed for simplicity and is not expected to significantly influence the reference solutions and multigroup data.

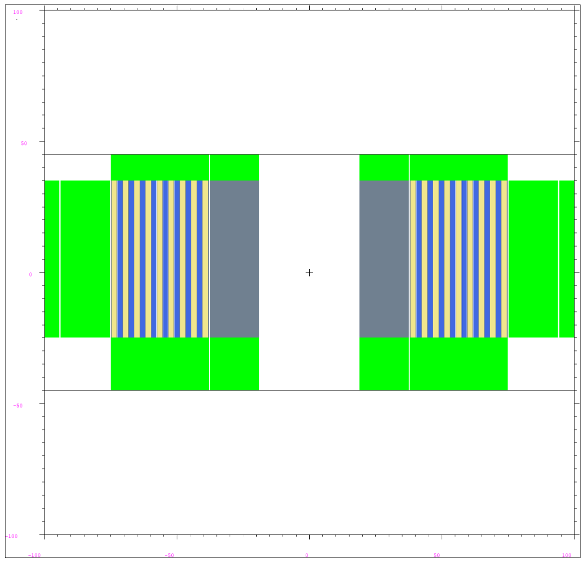

Figure 2 – XZ View of Core[1]

2.3 Assembly Geometric Specifications

The assembly lattice contains three types of non-void areas – containing fuel, control drums, or pure reflector.

2.3.1 Fuel Assembly

The fuel assembly is described as eight concentric rings surrounding a central heat pipe. The first-inner ring has six elements, the second-inner ring has twelve, etc. Odd-numbered rings are completely composed of moderator rods. The even-numbered rings alternate between fuel pins and heat pipes such that heat pipes are located at the corners.

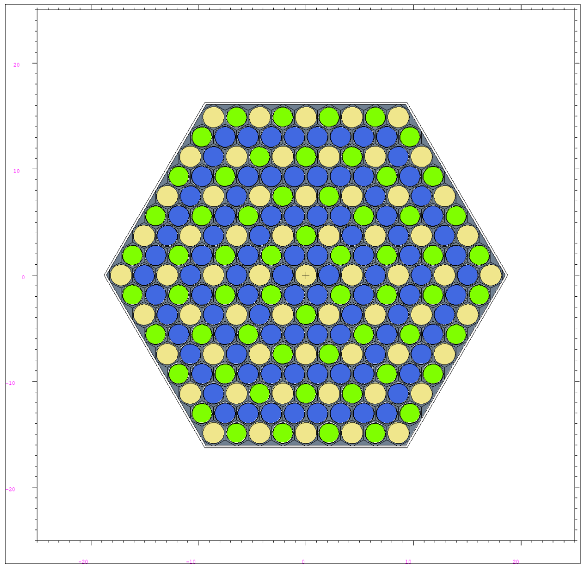

Figure 3 – XY View of Fuel Assembly[1]

Figure 3 depicts a 50 x 50 cm radial view and Figure 4 depicts a 100 x 100 cm axial view. In both figures, UN fuel is shown as lime green, YH_2 moderator as blue, heat pipes as tan, and surrounding stainless steel alloy 316 (SS316) monolith as gray.

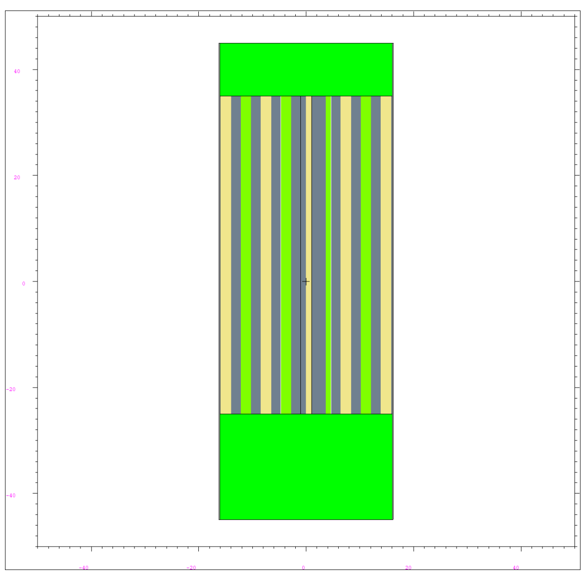

Figure 4 – YZ View of Fuel Assembly[1]

In the stylized model, heat pipes are modeled as a homogenization of an outer SS316 wall and the inner liquid-vapor sodium (Na) mixture[1]. A sufficient description of geometric specifications is noted in Table 2. Note that fuel pins and moderator rods leave a small gap between themselves and the surrounding monolith, which may not be seen in the above figures. However, heat pipes do contact the monolith.

Table 2 – Fuel Assembly Geometric Specifications[1]

Parameter	Value
Triangular pitch	2.15 cm
Fuel radius	0.925 cm
Fuel pin gap radius	0.05 cm
Moderator radius	0.95 cm
Moderator gap thickness	0.05 cm
Heat pipe radius	1.0 cm
Monolith apothem	16.0765 cm
Unit assembly pitch	32.553 cm
Unit assembly height	60 cm
Bottom reflector thickness	20 cm
Top reflector thickness	10 cm

2.3.2 Control Drum Assembly

The control drum assembly is a hexagonal block of beryllium containing a coaxial hole. Inside this hole is a beryllium cylinder containing a 90° arc of EuB_6 absorber, composing a control drum which maintains an equally spaced gap with the outside beryllium. This control drum can be rotated to change the criticality of the core. Details on this assembly are presented in Figure 5, and a 40 × 40 cm radial depiction of this block is shown in Table 3.

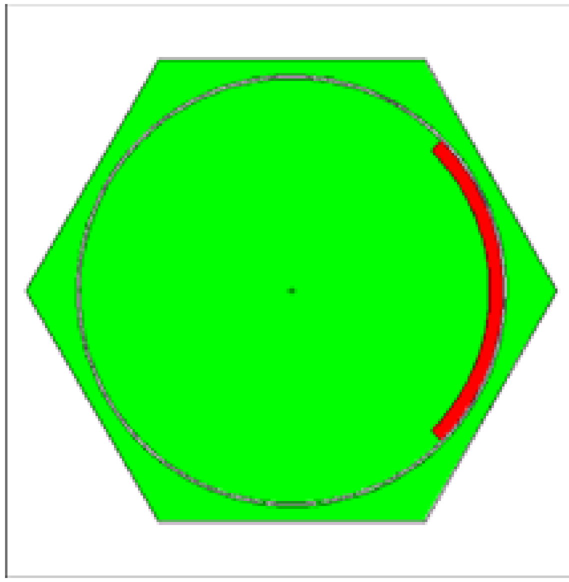

Figure 5 – XY View of Control Drum[1]

Table 3 – Control Drum Assembly Geometric Specifications[1]

Parameter	Value
Control drum hole radius	15 cm
Control drum radius	14.8 cm
Absorber outer radius	14.8 cm
Absorber inner radius	13.8 cm
Absorber thickness	1.0 cm
Absorber arc width	90°
Control drum height	60 cm

2.3.3 Reflector Block

The reflector blocks are those that cannot fit a full fuel assembly nor control drum – they are located at the outer boundaries of the core. The midpoint of each side of the core contains a trapezoidal block of pure beryllium and each corner of the core contains a pure beryllium block shaped as an equilateral triangle. These shapes are determined by the intersection of assembly lattice grids with the core periphery.

2.4 Temperature Specifications

The starting point of the temperature profile of this stylized design comes from a thermal hydraulic analysis presented in the literature[3], which describes maximum, average, and minimum temperatures in materials native to the active region of the fuel assembly (UN, YH2, heat pipes, and monolith) as shown in Table 4 (taken from Table IV of Reference 3). The gap in beryllium and EuB_6 absorber temperature is closed by assuming at temperature of 600 K for all instances of both materials. Placing the outer materials of the core at the midpoint between presumed room temperature and assembly material temperatures is a plausible assumption, and SERPENT 2 contains cross section data evaluated at 600 K[4]. The reference solutions within are meant to benchmark across arbitrary Monte Carlo codes, and this choice of temperature removes a source of error caused by differing interpolation methods between cross section libraries at differing temperatures. Table 4 summarizes the material temperatures.

Table 4 – Uniform Material Temperatures

Material	Temp (K)
Monolith (SS316)[3]	937
Fuel (UN)[3]	951
Moderator (YH_2)[3]	964
Heat Pipe (SS316+Na)[3]	928
Reflector (Be)	600
Absorber (EuB_6)	600

In deciding on the temperatures of the fuel assembly materials, the authors of the thermal hydraulic analysis artificially fixed the moderator temperature to ensure a slightly negative effective temperature coefficient for the whole reactor. The temperatures of the other materials – fuel, monolith, and heat pipes – were allowed to change based on operating conditions. This process naturally leads to unphysical situations. However, these situations do not affect the principal goal of that paper in providing a test case for the DireWolf code[3]. The present thesis takes a similar approach as its purpose is to provide a set of benchmarks for the preparation of multigroup cross sections for neutronic applications. The only firm requirement is that the generated cross sections be suitable for testing neutronic transport and diffusion codes. Thus, by adopting the average temperatures for the assembly materials as given in the literature, the moderator average temperature is again assumed higher than the fuel average temperature. This obviously unphysical assumption still allows the generation of meaningful cross sections and testing of computational methods as this thesis demonstrates. However, for real applications such an assumption must be corrected via the use of realistic and plausible temperature profiles within the various materials throughout the fuel assembly. Such a revised exercise will be the subject of already proposed subsequent work.

2.5 Isotopic Compositions

Table 5 contains mass densities (ρ) and isotopic atomic densities used in this stylized design for the fuel, moderator, beryllium, and absorber. Atomic densities are written in units of nuclei per barn (b) per centimeter. These values are used in the units shown by the SERPENT 2 input files included with this thesis.

Table 5 – Atomic Density Data for Fuel, Moderator, Reflector, and Absorber[1]

Isotope	UN Fuel $\rho = 14.3$ g/cm^3	YH_2 Moderator $\rho = 4.3$ g/cm^3	Be Reflector $\rho = 1.854$ g/cm^3	EuB_6 Absorber $\rho = 4.895$ g/cm^3
^{1}H		5.69608×10^{-2}		
^{9}Be			1.23870×10^{-1}	
^{10}B				1.62323×10^{-2}
^{11}B				6.53371×10^{-2}
^{14}N	3.41086×10^{-2}			
^{15}N	1.36982×10^{-4}			
^{89}Y		2.84804×10^{-2}		
^{151}Eu				6.49972×10^{-3}
^{153}Eu				7.09518×10^{-3}
^{235}U	6.76350×10^{-3}			
^{238}U	2.74821×10^{-2}			

Table 6, in a similar fashion to Table 5, give the density data for the monolith and heat pipe. The wide variety of isotopes exclusive to these two materials necessitated the splitting of density data into two tables, especially as the heat pipe is modeled as a homogenization of sodium and monolith material (SS316).

Table 6 – Atomic Density Data for Heat Pipe and Monolith[1]

Isotope	SS316+Na Heat Pipe ρ = 2.267 g/cm^3	SS316 Monolith ρ = 7.9 g/cm^3
^{12}C		1.62484×10^{-4}
^{23}Na	4.92833×10^{-3}	
^{28}Si	4.11552×10^{-4}	7.92255×10^{-4}
^{29}Si	2.08976×10^{-5}	4.03864×10^{-5}
^{30}Si	1.37758×10^{-5}	2.66378×10^{-5}
^{31}P		3.53187×10^{-5}
^{32}S		2.11202×10^{-5}
^{33}S		1.66759×10^{-7}
^{34}S		9.44970×10^{-7}
^{36}S		2.56552×10^{-9}
^{50}Cr	1.77806×10^{-4}	6.76211×10^{-4}
^{52}Cr	3.42886×10^{-3}	1.30400×10^{-2}
^{53}Cr	3.88795×10^{-4}	1.47863×10^{-3}
^{54}Cr	9.67787×10^{-5}	3.68064×10^{-4}
^{55}Mn	4.56726×10^{-4}	8.78601×10^{-4}
^{54}Fe	8.58252×10^{-4}	3.33586×10^{-3}
^{56}Fe	1.34726×10^{-2}	5.23194×10^{-2}
^{57}Fe	3.11151×10^{-4}	1.20890×10^{-3}
^{58}Fe	4.14072×10^{-5}	1.14046×10^{-4}
^{58}Ni	1.74225×10^{-3}	6.62534×10^{-3}
^{60}Ni	6.71125×10^{-4}	2.55205×10^{-3}
^{61}Ni	2.91727×10^{-5}	1.10950×10^{-4}
^{62}Ni	9.30147×10^{-5}	3.53739×10^{-4}
^{64}Ni	2.36883×10^{-5}	9.01183×10^{-5}
^{92}Mo	4.83027×10^{-5}	1.81707×10^{-4}
^{94}Mo	3.01072×10^{-5}	1.13670×10^{-4}
^{95}Mo	5.18174×10^{-5}	1.96844×10^{-4}
^{96}Mo	5.42900×10^{-5}	2.06763×10^{-4}
^{97}Mo	3.10836×10^{-5}	1.18826×10^{-4}
^{98}Mo	7.85385×10^{-5}	2.92730×10^{-4}
^{100}Mo	3.13435×10^{-5}	1.20810×10^{-4}

CHAPTER 3. METHODOLOGY

From this stylized design, six benchmark problems are constructed with differing environmental effects arising from enforcement of assembly-wide boundary conditions or interaction between fuel and control drum assemblies. Four benchmark problems involve a single assembly. The first problem consists of a single assembly with its axial reflectors removed and the specular boundary condition invoked on the resulting geometry. This configuration is axially uniform and, due to the enforcement of the specular boundary condition at the top and bottom of the fueled portion of the assembly, can be treated as infinitely tall. For this reason, this problem will be known as the "2D assembly configuration" or "reference set" against which data from other benchmark problems will be compared to investigate the level of environmental effects experienced in the core.

Three benchmark problems involve a single assembly that retains its axial reflectors. These assemblies do vary axially and are modeled as finitely tall. Each of these assembly problems has different sets of boundary conditions enforced – one under pure vacuum (henceforth known as "3D Vacuum"), one under pure specular (henceforth known as "3D Specular"), and one under specular in the radial direction and vacuum in the axial direction (henceforth known as "3D Mixed").

The final two benchmark problems are full core configurations with all control drums rotated fully inwards or outwards, both of which under the vacuum boundary condition. Each of these six benchmark problems generates a different range of environmental effects within and across fuel assemblies and has been selected to study the effect of neutron leakage on multigroup data such as cross sections.

The previously detailed design is implemented in the continuous Monte Carlo code SERPENT 2[4]. Boundary conditions are selected, and cell definitions are modified to generate input files representing the six benchmark problems stated above. These input files are ran using the INL Sawtooth cluster, running at one million particles per cycle. An initialization series of one thousand inactive cycles follows the active series of ten thousand cycles where output is tallied. Each benchmark problem is run four times using continuous energy[6] and thermal scattering[7] libraries generated from the ENDF/B-VIII.0 data set. The first run of a benchmark problem calculates its reference solution – including eigenvalue and flux spectra – and multigroup macroscopic and microscopic data – including cross sections and nubar. The energy bins in which the multigroup data are tallied are separated by the CASMO 2-, 4-, and 8-group energy structures available in SERPENT 2[4] as presets, which are seen in Table 7.

Table 7 – Upper Bounds of Multigroup Energy Structures

<table>
<tr><th>8-Group</th><th>4-Group</th><th>2-Group</th></tr>
<tr><td>1.00×10^{1} MeV</td><td>1.00×10^{1} MeV</td><td rowspan="4">1.00×10^{1} MeV</td></tr>
<tr><td>8.21×10^{-1} MeV</td><td>8.21×10^{-1} MeV</td></tr>
<tr><td>5.53×10^{-3} MeV</td><td rowspan="2">5.53×10^{-3} MeV</td></tr>
<tr><td>4.00×10^{-6} MeV</td></tr>
<tr><td>6.25×10^{-7} MeV</td><td rowspan="4">6.25×10^{-7} MeV</td><td rowspan="4">6.25×10^{-7} MeV</td></tr>
<tr><td>2.80×10^{-7} MeV</td></tr>
<tr><td>1.40×10^{-7} MeV</td></tr>
<tr><td>5.80×10^{-8} MeV</td></tr>
</table>

The latter three runs of a benchmark problem homogenize each unique assembly and calculate the Legendre moments of the assemblies' scattering kernel up to third order, performed for each of the three energy group structures in Table 7. The number of machine-hours required to complete each run of each benchmark problem on the Sawtooth cluster with the above number of particles are shown in Table 8.

Table 8 – Computational Cost (CPU · hour) of Runs Performed

	Configurations	Reference Solution	Scattering Kernel		
			2-Group	**4-Group**	**8-Group**
Assembly	2D	1,938.0	3,110.1	2,386.9	1,846.6
	3D Specular	2,838.3	3,938.4	2,925.1	2,206.1
	3D Mixed	1,641.4	2,245.8	1,598.1	1,246.4
	3D Vacuum	1,484.8	2,055.8	1,541.1	1,164.3
Core	**Configurations**	**Reference Solution**	**2-Group**	**4-Group**	**8-Group**
	Drums-in	8,497.1	4,046.1	4,050.7	3,831.7
	Drums-out	9,112.5	4,394.5	5,343.1	4,772.3

The single fuel assembly as seen in Figure 3 shares the same symmetry characteristics as a hexagram – all six long radii from the center to each corner are lines of radial symmetry. Exactly between each long radius is a short radius or apothem, each of which is a line of reflectional symmetry. Thus, a one-twelfth slice of a fuel assembly bordered by a long radius and a short radius is the unique area of the assembly whose calculated data matches those of the other eleven up to rotation and reflection. Figure 6 shows a 18 × 18 cm radial view of one such slice divided by the y-positive apothem and long radius at a 60° angle. The pins are numbered by distance from the fuel assembly center then leftward from the long radius.

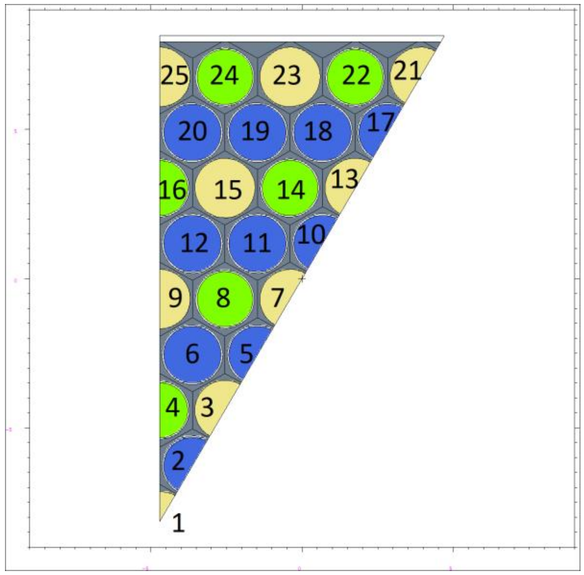

Figure 6 – XY View of Assembly Slice with Pin Numbering

The areas in which multigroup data are calculated are fuel pins 4, 8, 14, and 22; moderator rods 2 and 17; and heat pipes 1, 7, and 21. Note that lower indices for all materials represent regions closer to the assembly center and therefore provide a radial component to measuring the effect of such data on location within in the assembly. The regions listed are divided axially into five subregions of height 12 cm, labeled $z = 0 - 12$ cm, $z = 12 - 24$ cm, … $z = 48 - 60$ cm. Each such subregion has its multigroup data independently calculated.

The full core configurations also show hexagram-like symmetry like the single assembly; a similar slice of which is shown in Figure 7 depicting a 100 × 100 cm radial view. Note that the assembly slice shown in Figure 6 appears in the pieces of all three Assemblies (denoted A, B, and C) that compose the full core slice. In addition, the core slice contains the beryllium Block D in the shape of a right trapezoid, control drum assembly Block E, and beryllium Block F in the shape of an equilateral triangle.

Multigroup data calculation for full core benchmark problems is performed by dividing the core into 12-cm height regions as before. Each of the three fuel assemblies in a full core configuration is then evaluated as in a single assembly benchmark problem. Beryllium in each block and axial division is evaluated independent from one another. The absorber strip in the drum of Block E also has its data calculated.

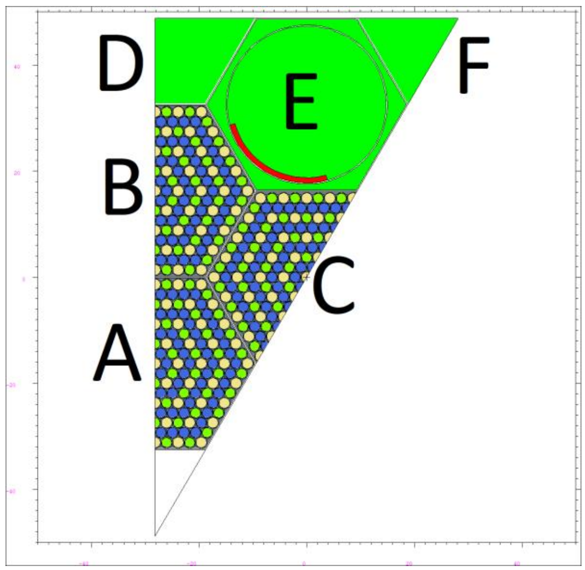

Figure 7 – XY View of Core Slice with Assembly Designation

Calculation of the reference solution of a benchmark problem includes its eigenvalue, normalized flux spectra averaged across its fuel and moderator, and fission rate density distribution. SERPENT 2 input files are configured to directly output multigroup reaction cross sections for a given region[4]. For each reaction, region, and energy group/bin (E_g), the cross section is evaluated as the reaction rate tally in the region volume (V) divided by the region's flux tally, both of which are sorted by the energy bin of the incident neutron. That is, the cross section ($\Sigma_{x,g}$) of reaction x in energy group g can be expressed as the ratio of two tallies in Equation 1:

$$\bar{\Sigma}_{x,g} = \frac{RR_{x,g}}{\phi_g} \tag{1}$$

where $RR_{x,g}$ is the reaction rate for reaction x in group g and ϕ_g is the cumulative scalar flux in group g. These tallies are discrete representations of integrals respectively defined in Equations 2 and 3:

$$RR_{x,g} = \int_V \int_{E_g} \Sigma_x(\vec{\mathbf{r}}, E)\phi(\vec{\mathbf{r}}, E) dE \; d^3\vec{\mathbf{r}} \tag{2}$$

$$\phi_g = \int_V \int_{E_g} \phi(\vec{\mathbf{r}}, E) dE \; d^3\vec{\mathbf{r}} \tag{3}$$

Included in the calculated multigroup data is the average number of neutrons produced per fission event (nubar, $\bar{\nu}$) in each region. Just as cross sections are averaged over flux within a region, the average nubar is weighed by the fission rate density in that region as seen in Equation 4:

$$\bar{\nu} = \frac{\int_V \int_{E_g} \nu(\vec{\mathbf{r}}, E)\Sigma_f(\vec{\mathbf{r}}, E)\phi(\vec{\mathbf{r}}, E) dE \; d^3\vec{\mathbf{r}}}{\int_V \int_{E_g} \Sigma_f(\vec{\mathbf{r}}, E)\phi(\vec{\mathbf{r}}, E) dE \; d^3\vec{\mathbf{r}}} \tag{4}$$

SERPENT 2 outputs reference solutions, multigroup data, and up-to-third-order Legendre moments of assembly-averaged scattering kernels, along with their respective one standard deviation (1σ) statistical uncertainties. Multigroup data are directly output in the 8-group structure in Table 7 and fewer-group statistics are calculated after the data run as the weighted flux average of all 8-group data contained in each coarse group. Statistical uncertainties involving multigroup data in fewer groups are calculated by performing uncertainty propagation on the sums of all 8-group reaction rates and fluxes within a coarser group. For example, Group 3 of 4 contains Groups 3 and 4 of 8 (see Table 5 which highlights the shared boundaries between energy structures), so the uncertainty $1\sigma(\phi_{3/4})$[a] of flux in Group 3 of 4 is calculated as in Equation 5:

$$1\sigma(\phi_{3/4}) = \sqrt{1\sigma^2(\phi_{3/8}) + 1\sigma^2(\phi_{4/8})} \tag{5}$$

Once $RR_{x,g}$ and ϕ_g have their respective uncertainties $1\sigma(RR_{x,g})$ and $1\sigma(\phi_g)$ calculated, the uncertainty of the cross section $1\sigma(\bar{\Sigma}_{x,g})$ is calculated as in Equation 6:

$$1\sigma(\bar{\Sigma}_{x,g}) = \bar{\Sigma}_{x,g}\sqrt{\left(\frac{1\sigma(RR_{x,g})}{RR_{x,g}}\right)^2 + \left(\frac{1\sigma(\phi_g)}{\phi_g}\right)^2} \tag{6}$$

These uncertainty propagation formulas assume an independence between ϕ_g and $RR_{x,g}$, itself a function of flux as seen in Equation 2. Therefore, the uncertainties in multigroup data reported in this thesis are overestimates as the correlation between these two values is ignored.

Investigation of differing environmental effects throughout each benchmark problem is performed by comparing multigroup data of that benchmark problem against the respective data of the 2D assembly problem generated as a reference. These comparisons are reported as the percent error incurred (PEI) in using data generated from

[a] The notation *n*σ denotes *n* times statistical uncertainty, and is used to disambiguate from microscopic cross section, which is never preceded by a number.

the 2D reference problem, such as a cross section (Σ_{2D}) to approximate the true data (Σ) of a benchmark problem, as seen in Equation 7:

$$PEI = \left(\frac{\Sigma_{2D} - \Sigma}{\Sigma}\right)(100\%) \tag{7}$$

If PEI is negative, that means the 2D approximation underestimates the true cross section or nubar and that this true value is higher than its counterpart in the 2D reference case. Likewise, a positive PEI describes an overestimation of the true cross section by the 2D approximation.

CHAPTER 4. RESULTS AND CONCLUSIONS

This chapter highlights selections of calculated results for each of the six benchmark problems. All problems are modeled using the continuous energy Monte Carlo code SERPENT 2[4]. The full set of data include for each benchmark problem its reference solution (eigenvalue, flux spectrum, and fission rate density distribution); multigroup cross section distribution for radiative capture (reactions consuming a neutron and that do not produce neutrons), scattering, fission, the (n, 2n) reaction, and in total; multigroup nubar distribution; and multigroup Legendre moments up to third order of scattering kernels averaged across each assembly. All multigroup data are output in the 8-group energy bin structure as seen in Table 7. Multigroup cross sections and nubars are processed into the 2- and 4-group structures after the initial run detailed in CHAPTER 3. The next three runs directly output the Legendre moments.

All multigroup data in the initial run are presented in this chapter as a function of, as applicable, assembly notation, pin number (representing radial distance from some center point depending on benchmark problem) and axial location. This set of data contains SERPENT 2 input and output files and tables of post-processed multigroup data and is not practical to include in the text of the thesis. However, the set is available as supplementary data attached to this thesis for the purposes of benchmarking approximations to transport in varying boundary conditions. These approximations include diffusion theory and the use of two-step methods where assemblies in the first step are modeled under the specular boundary condition. For benchmarking these approximations, Appendix A includes an example and description for the input file for the 2D assembly case.

The goal of this chapter is to report reference solutions and showcase multigroup data of interest, but to more importantly compare cross sections generated by 3D analysis of a single assembly or whole core configuration against those generated by the 2D single assembly. The following comparisons will investigate the effect of core environment on cross sections and their divergence from those generated from the industry-standard 2D single lattice transport method without influence from reflectors, control material, or outside elements.

4.1 Reference Solutions

The reference solutions reported in this section include eigenvalues, pin fission distributions, and flux spectra in fuel and moderator for all six benchmark problems.

4.1.1 Eigenvalues

Table 9 contains the calculated eigenvalues of each benchmark problem. The eigenvalues within behave as expected, with higher neutron reflection back into the core yielding higher criticalities for 3D problems. The 2D k_{eff} is lowered due to the lack of thermalizing beryllium between "copies" of the assembly generated by the specular boundary condition.

Table 9 – Benchmark Problem Eigenvalues

	Configurations	Eigenvalue (± 1σ, pcm)
Assembly	2D Assembly	1.24977 ± 0.4
	3D Specular	1.25504 ± 0.5
	3D Mixed	1.18063 ± 0.5
	3D Vacuum	0.60038 ± 1.4
Core	**Configurations**	**Eigenvalue**
	Drums-in	1.08374 ± 0.6
	Drums-out	1.10647 ± 0.6

4.1.2 Fission Rate Distributions

Table 10 contains the normalized fission rate distribution within each single assembly boundary condition configuration. This table is structured so that increasing radial distance from the center is shown from left to right (represented by increasing fuel pin indices) and the top of each assembly is represented by the top 12-cm range of each subregion of the table. This table normalizes its values by the volume of all fuel pins in each assembly (and therefore problem set) so that the average value for each is one.

Table 10 – Normalized Pin Fission Distributions for Assembly Configurations

Configuration	Data	Normalized Pin Fission Rates (% 1σ)			
	z (cm)	Pin 04	Pin 08	Pin 14	Pin 22
2D Reference	0-60	1.159 (0.01)	1.106 (0.01)	1.032 (0.01)	0.703 (0.01)
3D Specular	48-60	1.480 (0.02)	1.422 (0.02)	1.350 (0.02)	1.023 (0.02)
	36-48	1.059 (0.02)	1.010 (0.02)	0.943 (0.02)	0.644 (0.02)
	24-36	1.003 (0.02)	0.956 (0.02)	0.892 (0.02)	0.609 (0.02)
	12-24	0.960 (0.02)	0.916 (0.02)	0.855 (0.02)	0.585 (0.02)
	0-12	1.204 (0.02)	1.157 (0.02)	1.098 (0.02)	0.832 (0.02)
3D Mixed	48-60	0.889 (0.02)	0.850 (0.02)	0.796 (0.02)	0.561 (0.03)
	36-48	1.092 (0.02)	1.041 (0.02)	0.968 (0.02)	0.660 (0.02)
	24-36	1.245 (0.02)	1.185 (0.02)	1.103 (0.02)	0.751 (0.02)
	12-24	1.246 (0.02)	1.187 (0.02)	1.105 (0.02)	0.753 (0.02)
	0-12	1.300 (0.02)	1.245 (0.02)	1.172 (0.02)	0.854 (0.02)
3D Vacuum	48-60	1.283 (0.02)	1.008 (0.03)	0.639 (0.03)	0.214 (0.05)
	36-48	1.724 (0.02)	1.356 (0.02)	0.863 (0.03)	0.293 (0.04)
	24-36	1.929 (0.02)	1.517 (0.02)	0.966 (0.03)	0.328 (0.04)
	12-24	1.784 (0.02)	1.403 (0.02)	0.894 (0.03)	0.303 (0.04)
	0-12	1.428 (0.02)	1.122 (0.02)	0.709 (0.03)	0.237 (0.05)

The fission macroscopic cross section generally decreases with increasing incident neutron energy, and vice versa. Placing axial reflectors on top and bottom of the 2D case thermalizes neutrons reflected to the core, increasing the chance of fission. In the 3D specular case, neutrons must travel farther bottomward than topward to reach moderator and fuel, resulting in a higher fission rate at the top. But, removing the axial specular boundary condition to make the 3D mixed case increases leakage more at the top than at the bottom, creating a higher fission rate at the bottom. Finally, the 3D vacuum case has a harder flux at the periphery due to less surrounding moderator, so the fission rate greatly decreases at that location.

Table 11 contains the normalized fission rate distribution for the drums-in core configuration within all three Assemblies A, B, and C as shown in Figure 7.

Table 11 – Normalized Pin Fission Distribution for Drums-in Core Configuration

Configuration	**Data**	**Normalized Pin Fission Rates (% 1σ)**			
	z (cm)	Pin 04	Pin 08	Pin 14	Pin 22
Assembly A	48-60	0.955 (0.08)	0.893 (0.08)	0.807 (0.09)	0.543 (0.11)
	36-48	1.161 (0.07)	1.086 (0.07)	0.975 (0.08)	0.635 (0.09)
	24-36	1.303 (0.07)	1.218 (0.07)	1.095 (0.07)	0.713 (0.09)
	12-24	1.283 (0.07)	1.201 (0.07)	1.079 (0.07)	0.701 (0.09)
	0-12	1.289 (0.07)	1.212 (0.07)	1.098 (0.08)	0.754 (0.09)
Assembly B	48-60	1.079 (0.13)	0.847 (0.15)	0.643 (0.18)	0.449 (0.22)
	36-48	1.368 (0.11)	1.104 (0.13)	0.889 (0.15)	0.730 (0.17)
	24-36	1.547 (0.10)	1.250 (0.12)	1.013 (0.14)	0.843 (0.15)
	12-24	1.496 (0.10)	1.200 (0.12)	0.960 (0.14)	0.785 (0.16)
	0-12	1.394 (0.11)	1.074 (0.13)	0.792 (0.16)	0.537 (0.20)
Assembly C	48-60	1.102 (0.11)	0.856 (0.13)	0.639 (0.16)	0.441 (0.20)
	36-48	1.381 (0.10)	1.101 (0.11)	0.866 (0.13)	0.703 (0.15)
	24-36	1.558 (0.09)	1.246 (0.10)	0.985 (0.12)	0.811 (0.14)
	12-24	1.517 (0.09)	1.204 (0.10)	0.941 (0.12)	0.759 (0.14)
	0-12	1.448 (0.10)	1.108 (0.11)	0.802 (0.14)	0.531 (0.18)

Table 12 contains the normalized fission rate distribution for the drums-out core configuration within all three Assemblies A, B, and C as shown in Figure 7.

Table 12 – Normalized Pin Fission Distribution for Drums-out Core Configuration

Configuration	Data	Normalized Pin Fission Rates (% 1σ)			
	z (cm)	Pin 04	Pin 08	Pin 14	Pin 22
2D Reference	0-60	1.159 (0.01)	1.106 (0.01)	1.032 (0.01)	0.703 (0.01)
Assembly A	48-60	0.935 (0.09)	0.891 (0.09)	0.822 (0.10)	0.566 (0.11)
	36-48	1.134 (0.08)	1.081 (0.08)	0.993 (0.08)	0.663 (0.10)
	24-36	1.270 (0.07)	1.212 (0.07)	1.114 (0.08)	0.743 (0.09)
	12-24	1.247 (0.07)	1.188 (0.08)	1.089 (0.08)	0.726 (0.09)
	0-12	1.252 (0.08)	1.196 (0.08)	1.102 (0.08)	0.776 (0.10)
Assembly B	48-60	0.923 (0.12)	0.775 (0.13)	0.653 (0.15)	0.582 (0.16)
	36-48	1.202 (0.10)	1.044 (0.11)	0.955 (0.12)	1.011 (0.12)
	24-36	1.358 (0.09)	1.194 (0.10)	1.096 (0.11)	1.179 (0.11)
	12-24	1.290 (0.09)	1.116 (0.10)	1.014 (0.11)	1.067 (0.12)
	0-12	1.155 (0.11)	0.947 (0.12)	0.775 (0.14)	0.665 (0.15)
Assembly C	48-60	0.904 (0.11)	0.766 (0.12)	0.655 (0.13)	0.603 (0.14)
	36-48	1.160 (0.09)	1.028 (0.10)	0.955 (0.10)	1.051 (0.10)
	24-36	1.314 (0.08)	1.170 (0.09)	1.095 (0.09)	1.227 (0.09)
	12-24	1.257 (0.09)	1.104 (0.09)	1.018 (0.10)	1.112 (0.10)
	0-12	1.150 (0.09)	0.951 (0.10)	0.788 (0.12)	0.694 (0.13)

The trends of pin fission distributions in Assembly A as seen in Table 11 (drums-in) and Table 12 (drums-out) crudely match those of the 3D mixed single assembly seen in Table 10, due to Assembly A's position near the center of the core and the use of the vacuum boundary condition for core configurations. This is especially true for the drums-out configuration due to having its absorber farther away from Assembly A. However, the fission rate distributions in Assembly A for either core configuration cannot be approximated by those in the 2D assembly case, or any assembly case for that matter. Fission rate distributions in Assemblies B and C do not seem to match those in any assembly case. This is due to the presence of neighboring beryllium blocks on two sides of either Assembly, an environmental effect not accounted for in the assembly cases.

4.1.3 Flux Spectra

Figure 8 contains the normalized flux spectrum averaged across all fuel material in single assembly cases. This spectrum is normalized such that its integration over lethargy is equal to one and represents the energy decrease from an average scattering event as an equal move leftward independent of incident neutron energy. This mode of depiction also highlights flux hardenings and softenings as proportions to the entire spectrum.

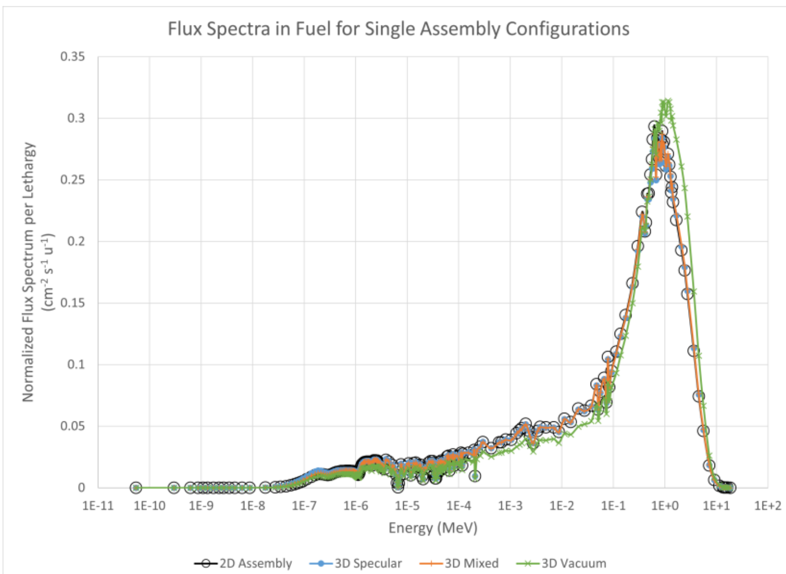

Figure 8 – Normalized Fuel Flux Spectrum for Selected Assembly Configurations

In the figure above, the fuel flux spectrum remains fast for all assembly boundary condition sets. As expected, the spectrum hardens with increasing leakage enforced by changing the boundary condition, especially in the 3D vacuum single assembly case.

Figure 9 contains the normalized flux spectrum averaged across all moderator material in all single assembly cases.

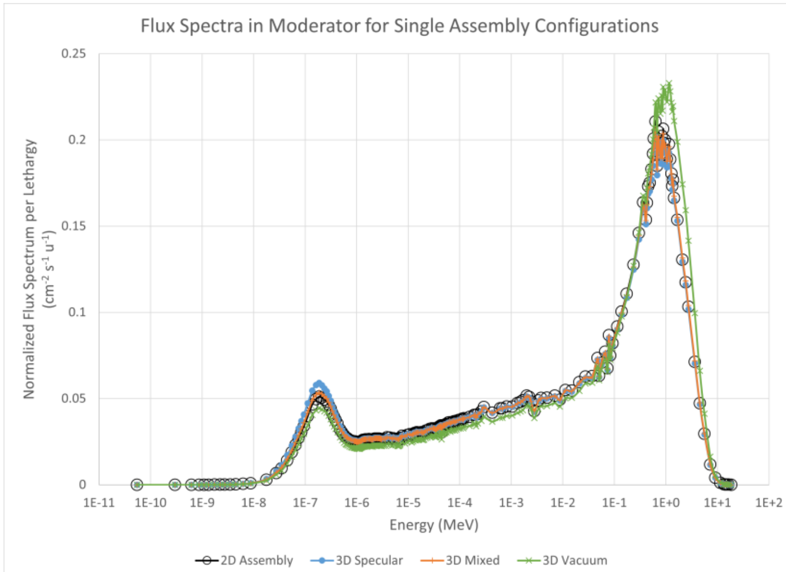

Figure 9 – Normalized Moderator Flux Spectrum for Selected Assembly Configurations

As expected, the flux spectrum in the moderator softens to form a thermal peak. Thermalization is greatest in the 3D specular case because of the beryllium axial reflectors and is lowest in the 3D vacuum case due to high leakage.

Figure 10 contains the normalized flux spectrum averaged across all fuel material in Assembly B of both core configurations. This fuel assembly showed more difference than Assemblies A and C of flux spectra caused by drum rotation.

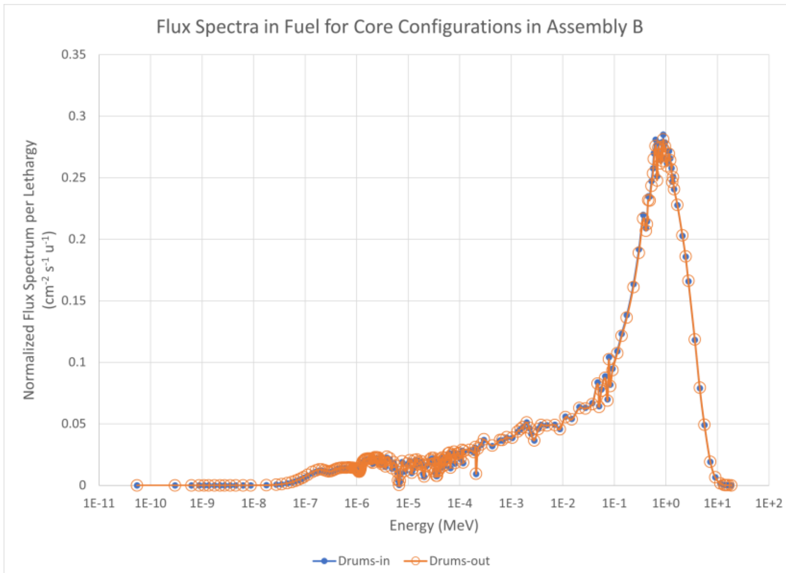

Figure 10 – Normalized Fuel Flux Spectrum in Assembly B for Core Configurations

The core flux spectrum resembles that of the 3D mixed case due to the core configuration containing the presence of multiple radially contacting fuel assemblies and the allowance of neutrons to leak out axially.

Figure 11 contains the normalized flux spectrum averaged across all fuel material in Assembly B of both core configurations.

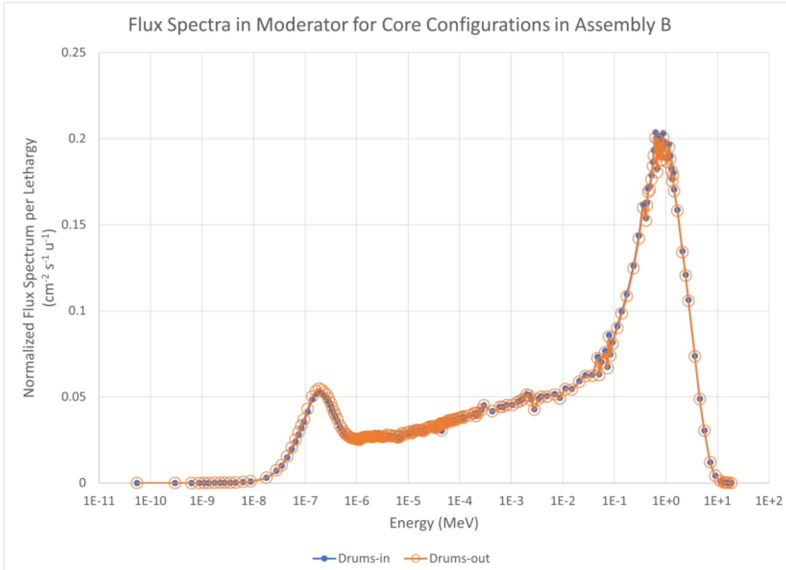

Figure 11 – Normalized Moderator Flux Spectrum in Assembly B for Core Configurations

As seen in Figure 10 and Figure 11, rotating the drums inward slightly hardens the flux, especially near the fast peak. This effect is caused by the absorber strip moving closer to the fuel assemblies in a position where more neutrons have not yet been reflected by the surrounding beryllium.

4.2 Two-Group Macroscopic Data for 2D Single Assembly

This section contains macroscopic data in the two-group structure as seen in Table 7 as a function of radial position with the 2D single assembly benchmark problem. These groups may be named as "thermal" for the group below 625 millielectronvolts (meV) and "fast" for the group above this threshold. Because the problem is axially uniform and the specular boundary condition is enforced, no effect is created by axial position. The following data are formatted as tables describing the effect of radial position on macroscopic cross sections and, if applicable, nubar on the three different elements embedded within the assembly's monolith: fuel pins (#4, #8, #14, #22), moderator rods (#2, #17), and heat pipes (#1, #7, #21). An increasing index represents an element farther away from the center of the assembly.

These data are presented in this section to establish a reference against which multigroup data from other benchmark problem sets are compared to investigate the presence of differing environmental effects in each problem. Microscopic two-group data for this problem are detailed in Appendix C for the sake of completeness and brevity of this section.

4.2.1 Fast Data

Table 13 contains fast (E > 625 meV) group macroscopic cross sections and nubars in fuel pins #4, #8, #14, and #22 for the 2D single assembly case.

Table 13 – Macroscopic Data for Fuel Rods in 2D Assembly Configuration, Group 1 of 2

Location / Data (% 1σ)	Pin 04	Pin 08	Pin 14	Pin 22
Total Σ (cm^{-1})	2.242 (0.02)	2.233 (0.02)	2.226 (0.02)	2.166 (0.03)
Capture Σ (cm^{-1})	0.2931 (0.02)	0.2914 (0.02)	0.2902 (0.02)	0.2792 (0.03)
Scatter Σ (cm^{-1})	0.6750 (0.02)	0.6751 (0.02)	0.6751 (0.02)	0.6755 (0.03)
Fission Σ (cm^{-1})	1.274 (0.02)	1.266 (0.02)	1.261 (0.02)	1.211 (0.02)
Nubar	2.432 (0.02)	2.432 (0.02)	2.432 (0.02)	2.432 (0.03)

It is seen in Table 13 that all fast fuel cross sections are significantly dependent on radial position, especially at the assembly periphery at fuel pin #22 where the cross section is lower. Nubar at pins #14 and #22 are statistically different from that at pin #4.

Table 14 contains fast group macroscopic cross sections in moderator rods #2 and #17 for the 2D single assembly case.

Table 14 – Macroscopic Data for Moderator Rods in 2D Assembly Configuration, Group 1 of 2

Location / Data (% 1σ)	Rod 02	Rod 17
Total Σ (cm^{-1})	1.983 (0.01)	1.970 (0.01)
Capture Σ (cm^{-1})	0.02483 (0.02)	0.02448 (0.02)
Scatter Σ (cm^{-1})	1.958 (0.01)	1.945 (0.02)

It is seen in Table 14 that all fast moderator cross sections are higher in moderator rod #2 closer to the center than in rod #17 closer to the periphery.

Table 15 contains fast group macroscopic cross sections in heat pipes #1, #7, and #1 for the 2D single assembly case.

Table 15 – Macroscopic Data for Heat Pipes in 2D Assembly Configuration, Group 1 of 2

Location / Data (% 1σ)	HP 01	HP 07	HP 21
Total Σ (cm^{-1})	0.2770 (0.02)	0.2755 (0.03)	0.2732 (0.06)
Capture Σ (cm^{-1})	0.03096 (0.03)	0.02966 (0.03)	0.02757 (0.06)
Scatter Σ (cm^{-1})	0.2461 (0.02)	0.2459 (0.03)	0.2456 (0.06)

It is seen in Table 15 that all fast heat pipe cross sections are significantly dependent on radial position, especially at the assembly periphery at heat pipe #21.

4.2.2 Thermal Data

Table 16 contains thermal (E < 625 meV) group macroscopic cross sections and nubars in fuel pins #4, #8, #14, and #22 for the 2D single assembly case.

Table 16 – Macroscopic Data for Fuel Rods in 2D Assembly Configuration, Group 2 of 2

Location / Data (% 1σ)	Pin 04	Pin 08	Pin 14	Pin 22
Total Σ (cm^{-1})	0.5560 (0.01)	0.5562 (0.01)	0.5557 (0.01)	0.5336 (0.01)
Capture Σ (cm^{-1})	0.03155 (0.01)	0.03120 (0.01)	0.03050 (0.01)	0.02524 (0.01)
Scatter Σ (cm^{-1})	0.4416 (0.01)	0.4429 (0.01)	0.4446 (0.01)	0.4322 (0.01)
Fission Σ (cm^{-1})	0.03759 (0.01)	0.03708 (0.01)	0.03612 (0.01)	0.03045 (0.01)
Nubar	2.525 (0.01)	2.524 (0.01)	2.521 (0.01)	2.519 (0.01)

Table 16 shows that capture and fission cross sections are statistically dependent on radial position within the assembly, enough so to render the total cross section as a function of radial position. Scattering cross section and nubar are statistically identical throughout the assembly.

Table 17 contains thermal group macroscopic cross sections in moderator rods #2 and #17 for the 2D single assembly case.

Table 17 – Macroscopic Data for Moderator Rods in 2D Assembly Configuration, Group 2 of 2

Location / Data (% 1σ)	Rod 02	Rod 17
Total Σ (cm^{-1})	0.8924 (0.01)	0.8758 (0.01)
Capture Σ (cm^{-1})	0.0009192 (0.01)	0.0008040 (0.02)
Scatter Σ (cm^{-1})	0.8867 (0.01)	0.8706 (0.01)

It is seen in Table 17 that all thermal moderator cross sections are higher in moderator rod #2 closer to the center than in rod #17 closer to the periphery.

Table 18 contains thermal group macroscopic cross sections in heat pipes #1, #7, and #1 for the 2D single assembly case.

Table 18 – Macroscopic Data for Heat Pipes in 2D Assembly Configuration, Group 2 of 2

Location / Data (% 1σ)	HP 01	HP 07	HP 21
Total Σ (cm^{-1})	0.1783 (0.01)	0.1703 (0.01)	0.1536 (0.01)
Capture Σ (cm^{-1})	0.001390 (0.02)	0.001195 (0.02)	0.0008555 (0.03)
Scatter Σ (cm^{-1})	0.1723 (0.01)	0.1642 (0.01)	0.1477 (0.01)

Table 18 shows that scattering cross section is not statistically dependent on radial position, but capture cross section is. The dependence on location of the capture cross section renders the total cross section statistically dependent on location as well.

4.2.3 Discussion

To aid in understanding the behavior of cross sections and nubar as a function of position within the 2D assembly, Figure 12 contains a XY view of a portion of the infinite lattice of fuel assemblies generated by the enforcement of the specular boundary condition on the 2D assembly (and the 3D specular assembly). Figure 12 also numbers (as done in CHAPTER 3) the regions that have their multigroup data calculated, either directly or indirectly via reflection, rotation, or translation of a directly calculated region.

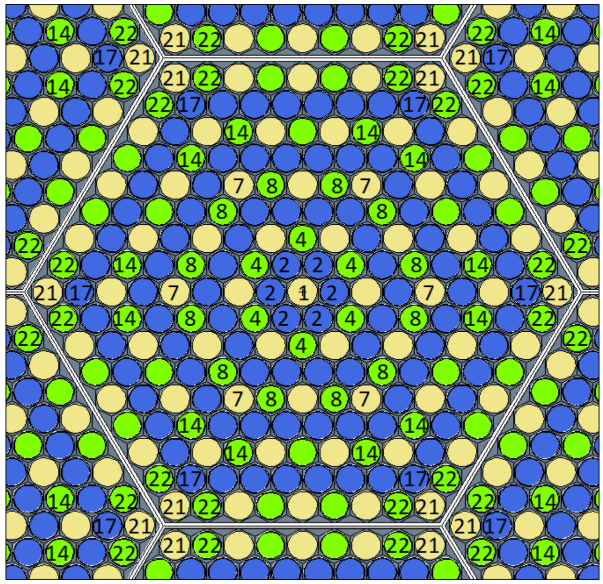

Figure 12 – Infinite Assembly Lattice with Pin Numbering

As seen in Figure 12, fuel pins #4, #8, and #14 immediately neighbors four moderator rods, but fuel pin #22 at the periphery only neighbors two. In addition, heat pipe #1 is surrounded by six moderator rods, heat pipe #7 neighbors four moderator rods, and heat pipe #21 neighbors only one. Moderator rods serve to thermalize and soften the flux, and the higher concentration of these rods in the center of the assembly yields a softer flux spectrum at the center and a harder flux spectrum at the periphery.

Cross sections generally decrease with increasing neutron energy and hardening flux spectrum. This results in higher cross sections in both groups in the center than at the peripheries. One exception is in the thermal scattering cross section – this cross section as a function of energy tends to remain constant as a function of energy in the thermal region, yielding a lack of dependence on radial position as seen in the tables in Chapter 4.2.2. The other exception lies in the fast nubar and (n, *n) cross section, which only substantially increase (the latter from zero) beginning at an energy on the order of several MeV – much higher than the two-group energy cutoff. Neutrons with these energies typically have not scattered yet and therefore have just been born from fission processes. As seen in the pin fission distributions in Chapter 4.1 and the thermal fission cross section distributions in Chapter 4.2.2, more fission events occur in the center than at the periphery, and therefore more interaction occurs in the center, yielding higher values for fast nubar and the (n, *n) cross section.

4.3 Four-Group Scattering Kernels for 2D Single Assembly

The tables in this section contain the four-group P_0 – P_3 Legendre moments of the scattering kernels averaged over the 2D single assembly. Each Legendre moment is represented as a 4x4 matrix and is written such that the element in row g' and column g represents the macroscopic cross section of a neutron whose incident energy is in energy group g' of 4 scattering to energy group g of 4, abbreviated as $\Sigma_{s,g'\to g}$. Legendre moments for other benchmark problem sets are included in supplemental data.

4.3.1 Legendre Moments

Table 19 contains the four-group isotropic P_0 Legendre moment averaged over the 2D single assembly.

Table 19 – Four-Group P_0 Macroscopic Scattering Kernel Averaged Over 2D Assembly Configuration

$\Sigma_{s,g'\to g}$ (cm^{-1}, % 1σ) g′ ↓ g →	1	2	3	4
1	1.781E-1 (0.001)	5.594E-2 (0.001)	2.189E-4 (0.020)	1.387E-8 (2.390)
2	0	4.347E-1 (0.001)	3.671E-2 (0.001)	3.621E-6 (0.111)
3	0	0	8.311E-1 (0.001)	3.193E-2 (0.001)
4	0	0	7.534E-3 (0.007)	1.194E-0 (0.001)

Table 20 contains the four-group linearly anisotropic P_1 Legendre moment averaged over the 2D single assembly.

Table 20 – Four-Group P_1 Macroscopic Scattering Kernel Averaged Over 2D Assembly Configuration

$\Sigma_{s,g'\to g}$ (cm^{-1}, % 1σ) g′ ↓ g →	1	2	3	4
1	7.226E-2 (0.001)	1.589E-2 (0.002)	1.078E-5 (0.064)	8.278E-9 (2.598)
2	0	1.363E-1 (0.001)	1.471E-2 (0.001)	3.434E-7 (0.458)
3	0	0	2.651E-1 (0.001)	9.547E-3 (0.003)
4	0	0	2.216E-3 (0.015)	2.996E-1 (0.002)

Table 21 contains the four-group second order P_2 Legendre moment averaged over the 2D single assembly.

Table 21 – Four-Group P_2 Macroscopic Scattering Kernel Averaged Over 2D Assembly Configuration

$\Sigma_{s,g'\to g}$ (cm^{-1}, % 1σ) g′ ↓ g →	1	2	3	4
1	5.143E-2 (0.001)	6.824E-4 (0.039)	-1.007E-4 (0.021)	2.000E-9 (7.389)
2	0	5.949E-2 (0.001)	-4.452E-3 (0.003)	-9.917E-7 (0.164)
3	0	0	1.054E-1 (0.001)	-1.987E-3 (0.010)
4	0	0	8.558E-4 (0.027)	9.488E-2 (0.003)

Table 22 contains the four-group third order P_3 Legendre moment averaged over the 2D single assembly.

Table 22 – Four-Group P_3 Macroscopic Scattering Kernel Averaged Over 2D Assembly Configuration

$\Sigma_{s,g'\to g}$ (cm^{-1}, % 1σ) g′ ↓ g →	1	2	3	4
1	2.818E-2 (0.002)	-6.986E-3 (0.004)	-1.755E-5 (0.032)	-1.088E-9 (12.29)
2	0	1.059E-2 (0.006)	-9.347E-3 (0.001)	-1.992E-7 (0.633)
3	0	0	8.723E-3 (0.011)	-3.079E-3 (0.006)
4	0	0	7.291E-5 (0.262)	3.120E-2 (0.008)

4.3.2 *Discussion*

As expected, most scattering events occur within the same originating group. Increasing scattering cross section with decreasing neutron energy (and therefore increasing group number) can be seen in all four kernels, although this relationship somewhat deteriorates with increasing order. Fast-to-thermal scattering events (increasing group number), while relatively uncommon, do occur – the group number can increase from any number to any higher number due to the presence of hydrogen within the moderator. Thermal-to-fast scattering events (decreasing group number) only significantly occur from group 4 to group 3 when the neutron crosses the 625 meV threshold – several times higher than the thermal peak seen in moderator flux spectra found in Chapter 4.1.3.

4.4 Selected Two-Group Macroscopic Data in Core Configurations

This section contains macroscopic fast scattering cross sections of beryllium blocks D, E, and F (see Figure 7) as well as macroscopic thermal cross sections of the EuB_6 absorber in Block E in both core configurations. Such blocks contain no fissionable material and therefore cannot be modeled by the 2D single assembly or any variant of the industry standard lattice depletion method. Nevertheless, an investigation of core environmental effects on nonfissionable elements of the core is merited as there is no preclusion that the performance of these control materials is not a function of the assemblies these materials control. The data in this section are therefore included to provide a benchmark for elements in the core not included by the 2D single assembly.

4.4.1 *Beryllium Fast Macroscopic Scattering Cross Sections*

Table 23 contains fast group macroscopic scattering cross sections in control Blocks D, E, and F for both core configurations.

Table 23 – Macroscopic Scattering Cross Sections for Beryllium in Core Configurations, Group 1 of 2

z (cm)	Drums-In Scatter Σ, cm^{-1} (% 1σ)		
	Block D	Block E	Block F
48-60	0.6497 (0.06)	0.6384 (0.04)	0.6835 (0.29)
36-48	0.6575 (0.04)	0.6477 (0.03)	0.7021 (0.23)
24-36	0.6578 (0.04)	0.6483 (0.03)	0.7030 (0.21)
12-24	0.6573 (0.04)	0.6474 (0.03)	0.7021 (0.22)
0-12	0.6491 (0.05)	0.6377 (0.04)	0.6832 (0.25)
z (cm)	Drums-Out Scatter Σ, cm^{-1} (% 1σ)		
	Block D	Block E	Block F
48-60	0.6501 (0.05)	0.6509 (0.03)	0.6693 (0.27)
36-48	0.6574 (0.04)	0.6582 (0.02)	0.6860 (0.21)
24-36	0.6577 (0.04)	0.6586 (0.02)	0.6867 (0.19)
12-24	0.6573 (0.04)	0.6581 (0.02)	0.6863 (0.21)
0-12	0.6498 (0.05)	0.6503 (0.03)	0.6712 (0.23)

4.4.2 *EuB_6 Thermal Macroscopic Absorption Cross Sections*

Table 24 contains thermal group macroscopic absorption cross sections in the EuB_6 absorber strip in Block E for both core configurations.

Table 24 – Macroscopic Capture Cross Sections for EuB_6 in Core Configurations, Group 2 of 2

z (cm)	Capture Σ, cm^{-1} (% 1σ)	
	Drums-In	Drums-Out
48-60	53.62 (0.05)	55.17 (0.06)
36-48	53.64 (0.04)	54.90 (0.04)
24-36	53.62 (0.04)	54.87 (0.03)
12-24	53.59 (0.04)	54.88 (0.04)
0-12	53.53 (0.05)	55.08 (0.05)

4.4.3 Discussion

Rotating the drums inward to outward does not have a significant effect on macroscopic scattering cross sections in beryllium Block D. Doing so in Block E significantly increases the cross section – this is due to the drum rotation placing more thermalizing beryllium between the fuel assemblies and the absorber strip, resulting in the flux spectrum softening to lower-energy regions with higher cross section. However, rotating the drums outward significantly decreases the cross section in Block F due to flux hardening. To explain, see in Figure 7 that a straight-line path from the core center to Block F requires going through the absorber strip in Block E. Given that the absorber strip has a high capture cross section at low energies, neutrons exit from the strip at high energies. The distance between the strip and Block F is lowest when the drums are rotated outward, which means less thermalization through beryllium, a harder flux spectrum entering Block F, and lower cross sections throughout.

If the drums are rotated inward, then the cross sections in Block E are significantly smaller than those in Block D. This effect is due to the absorber strip quickly removing low-energy neutrons that enter from the fuel assemblies, leaving a harder flux spectrum with lower scattering cross section. If the drums are rotated outward, then the strip is far enough away from the assemblies that the difference in cross sections between Blocks D and E is statistically insignificant. Regardless of drum rotation, Block F has significantly higher cross sections than Block D. This is due to neutrons being required to cross through Block E and potentially thermalize to reach Block F.

The thermal absorption cross section increases in the absorber strip upon rotating the drums outward. As stated before, doing so softens the flux to a region where the absorber is most effective.

4.5 Comparison of Core Configuration Data against 2D Single Assembly Data

This section investigates environmental effects in core configurations via comparison of regionwide cross sections between Assemblies A, B, and C in the drums-in and -out core configurations against those generated by analysis of the 2D single assembly. If core environmental effects cannot be ignored, then they will manifest as significant discrepancies between true multigroup data generated from whole core analysis and approximations thereof generated from an infinitely tall and perfectly reflecting typical assembly. Thus, these approximations which are inherent to the two-step lattice transport method must be corrected before being used by further core calculations.

The tables in this section contain macroscopic data in energy Group 2 of 8 – between 5.53 and 821 kiloelectronvolts (keV) – of the selected regions of elements in the 2D single assembly problem. This energy group was chosen as the contrast between cross sections generated for the whole core and those for the 2D single assembly was the greatest in this group for prevailing reactions within each material. Each region is paired with the three data of the corresponding region within each Assembly A, B, and C in each core configuration. To better illustrate the effect of core environment created by bordering material, the true data detailing the core assemblies are written as percents error incurred by using the 2D single assembly data to approximate the true data. A more detailed explanation of this method of presenting these data is given for Table 25 in Chapter 4.5.1, which shows the core environmental effect calculated as difference of group 2 of 8 macroscopic capture cross sections in fuel pins #4, #8, #14, and #22 incurred by using 2D assembly data to approximate the drums-in core configuration.

4.5.1 Macroscopic Capture Cross Sections

Table 25 – Error of Macroscopic Capture Cross Sections in Fuel Incurred by Using 2D Data to Approximate Drums-in Core Configuration, Group 2 of 8

Location		Error (% ± 1σ)		
Pin #	z (cm)	Assembly A	Assembly B	Assembly C
04[a]	48-60	-0.90 ± 0.12	-2.50 ± 0.18	-1.72 ± 0.16
	36-48	0.27 ± 0.11	-0.62 ± 0.16	-0.26 ± 0.14
	24-36	0.36 ± 0.11	-0.41 ± 0.16	0.01 ± 0.14
	12-24	0.30 ± 0.12	-0.29 ± 0.17	0.01 ± 0.15
	0-12	-0.57 ± 0.14	-1.66 ± 0.20	-1.01 ± 0.18
08[b]	48-60	-0.94 ± 0.12	-3.20 ± 0.20	-2.29 ± 0.18
	36-48	0.34 ± 0.11	-1.17 ± 0.18	-0.70 ± 0.16
	24-36	0.39 ± 0.11	-0.76 ± 0.17	-0.39 ± 0.15
	12-24	0.45 ± 0.12	-1.00 ± 0.18	-0.40 ± 0.17
	0-12	-0.56 ± 0.14	-2.38 ± 0.22	-1.79 ± 0.20
14[c]	48-60	-1.29 ± 0.12	-4.90 ± 0.23	-4.34 ± 0.21
	36-48	0.24 ± 0.11	-3.02 ± 0.20	-2.55 ± 0.18
	24-36	0.34 ± 0.11	-2.72 ± 0.19	-2.15 ± 0.17
	12-24	0.32 ± 0.12	-2.66 ± 0.21	-2.31 ± 0.19
	0-12	-0.64 ± 0.14	-4.28 ± 0.26	-3.24 ± 0.23
22[d]	48-60	-1.78 ± 0.12	-10.64 ± 0.27	-10.44 ± 0.24
	36-48	0.07 ± 0.11	-9.07 ± 0.22	-8.69 ± 0.20
	24-36	0.20 ± 0.11	-8.51 ± 0.21	-8.27 ± 0.20
	12-24	0.10 ± 0.12	-8.99 ± 0.23	-8.51 ± 0.21
	0-12	-1.40 ± 0.14	-10.09 ± 0.29	-9.52 ± 0.27

[a] 2D Σ (cm^{-1}): 0.009505 ± 0.01%
[b] 2D Σ (cm^{-1}): 0.009518 ± 0.01%
[c] 2D Σ (cm^{-1}): 0.009520 ± 0.01%
[d] 2D Σ (cm^{-1}): 0.009184 ± 0.01%

As an example, the capture cross section for group 2 of 8 in fuel pin #4 is 0.009505 cm^{-1} as approximated by the 2D case. This value is 1.01% lower than the capture cross section for the same group of the bottommost region of the same fuel pin in Assembly C of the drums-in core configuration, i.e., the capture cross section there is 0.009602 cm^{-1} as can be found in the supplemental data.

Table 26 shows the percent error of group 2 of 8 macroscopic capture cross sections in fuel pins #4, #8, #14, and #22 incurred by using 2D assembly data to approximate the drums-out core configuration.

Table 26 – Error of Macroscopic Capture Cross Sections in Fuel Incurred by Using 2D Data to Approximate Drums-out Core Configuration, Group 2 of 8

Location		Error (% ± 1σ)		
Pin #	z (cm)	Assembly A	Assembly B	Assembly C
04[a]	48-60	-1.20 ± 0.13	-2.09 ± 0.17	-1.79 ± 0.15
	36-48	0.10 ± 0.12	-0.42 ± 0.15	-0.12 ± 0.14
	24-36	0.11 ± 0.12	-0.26 ± 0.14	-0.12 ± 0.13
	12-24	0.14 ± 0.12	-0.36 ± 0.15	-0.13 ± 0.14
	0-12	-0.75 ± 0.15	-1.57 ± 0.19	-1.15 ± 0.17
08[b]	48-60	-1.34 ± 0.13	-2.67 ± 0.19	-1.90 ± 0.17
	36-48	0.07 ± 0.12	-0.88 ± 0.16	-0.39 ± 0.14
	24-36	0.10 ± 0.12	-0.70 ± 0.15	-0.27 ± 0.14
	12-24	0.12 ± 0.12	-0.59 ± 0.17	-0.34 ± 0.15
	0-12	-0.77 ± 0.14	-1.83 ± 0.20	-1.66 ± 0.18
14[c]	48-60	-1.49 ± 0.13	-3.78 ± 0.21	-3.18 ± 0.18
	36-48	-0.10 ± 0.12	-1.73 ± 0.17	-1.37 ± 0.15
	24-36	0.18 ± 0.12	-1.57 ± 0.16	-1.28 ± 0.15
	12-24	0.03 ± 0.12	-1.85 ± 0.18	-1.46 ± 0.16
	0-12	-0.98 ± 0.14	-3.38 ± 0.22	-2.58 ± 0.20
22[d]	48-60	-2.09 ± 0.13	-8.93 ± 0.23	-7.80 ± 0.21
	36-48	0.03 ± 0.12	-7.00 ± 0.18	-6.30 ± 0.16
	24-36	0.12 ± 0.12	-6.71 ± 0.17	-6.03 ± 0.16
	12-24	0.05 ± 0.12	-6.62 ± 0.19	-6.31 ± 0.17
	0-12	-1.62 ± 0.15	-8.28 ± 0.25	-7.39 ± 0.22

[a] 2D Σ (cm^{-1}): 0.009505 ± 0.01%
[b] 2D Σ (cm^{-1}): 0.009518 ± 0.01%
[c] 2D Σ (cm^{-1}): 0.009520 ± 0.01%
[d] 2D Σ (cm^{-1}): 0.009184 ± 0.01%

4.5.2 *Macroscopic Scattering Cross Sections*

Table 27 shows the percent error of group 2 of 8 macroscopic scattering cross sections in fuel pins #4, #8, #14, and #22 incurred by using 2D assembly data to approximate the drums-in core configuration.

Table 27 – Error of Macroscopic Scattering Cross Sections in Fuel Incurred by Using 2D Data to Approximate Drums-in Core Configuration, Group 2 of 8

Location		Error (% ± 1σ)		
Pin #	z (cm)	Assembly A	Assembly B	Assembly C
04[a]	48-60	-0.56 ± 0.11	-1.38 ± 0.16	-0.99 ± 0.14
	36-48	0.21 ± 0.10	-0.26 ± 0.15	-0.06 ± 0.13
	24-36	0.26 ± 0.10	-0.17 ± 0.14	0.07 ± 0.13
	12-24	0.25 ± 0.11	-0.15 ± 0.15	0.04 ± 0.14
	0-12	-0.33 ± 0.12	-0.92 ± 0.18	-0.66 ± 0.16
08[b]	48-60	-0.56 ± 0.11	-1.87 ± 0.18	-1.41 ± 0.16
	36-48	0.25 ± 0.10	-0.61 ± 0.16	-0.37 ± 0.14
	24-36	0.26 ± 0.10	-0.41 ± 0.16	-0.20 ± 0.14
	12-24	0.30 ± 0.11	-0.52 ± 0.17	-0.18 ± 0.15
	0-12	-0.32 ± 0.12	-1.30 ± 0.20	-1.01 ± 0.18
14[c]	48-60	-0.72 ± 0.11	-2.85 ± 0.21	-2.58 ± 0.18
	36-48	0.21 ± 0.10	-1.68 ± 0.18	-1.42 ± 0.16
	24-36	0.25 ± 0.10	-1.50 ± 0.17	-1.17 ± 0.16
	12-24	0.23 ± 0.11	-1.52 ± 0.19	-1.29 ± 0.17
	0-12	-0.37 ± 0.13	-2.38 ± 0.23	-1.90 ± 0.21
22[d]	48-60	-1.08 ± 0.11	-6.45 ± 0.24	-6.19 ± 0.22
	36-48	0.11 ± 0.10	-5.39 ± 0.20	-5.21 ± 0.18
	24-36	0.21 ± 0.10	-5.08 ± 0.19	-4.95 ± 0.18
	12-24	0.13 ± 0.11	-5.29 ± 0.21	-5.11 ± 0.19
	0-12	-0.82 ± 0.13	-6.05 ± 0.26	-5.72 ± 0.24

[a] 2D Σ (cm^{-1}): 0.4539 ± 0.01%
[b] 2D Σ (cm^{-1}): 0.4546 ± 0.01%
[c] 2D Σ (cm^{-1}): 0.4553 ± 0.01%
[d] 2D Σ (cm^{-1}): 0.4484 ± 0.01%

Table 28 shows the percent error of group 2 of 8 macroscopic scattering cross sections in fuel pins #4, #8, #14, and #22 incurred by using 2D assembly data to approximate the drums-out core configuration.

Table 28 – Error of Macroscopic Scattering Cross Sections in Fuel Incurred by Using 2D Data to Approximate Drums-out Core Configuration, Group 2 of 8

Location		Error (% ± 1σ)		
Pin #	z (cm)	Assembly A	Assembly B	Assembly C
04[a]	48-60	-0.73 ± 0.12	-1.26 ± 0.16	-1.03 ± 0.14
	36-48	0.11 ± 0.11	-0.19 ± 0.14	-0.07 ± 0.12
	24-36	0.12 ± 0.11	-0.12 ± 0.13	0.01 ± 0.12
	12-24	0.12 ± 0.11	-0.17 ± 0.14	0.00 ± 0.13
	0-12	-0.48 ± 0.13	-0.91 ± 0.17	-0.72 ± 0.16
08[b]	48-60	-0.79 ± 0.12	-1.52 ± 0.17	-1.14 ± 0.15
	36-48	0.08 ± 0.11	-0.41 ± 0.14	-0.17 ± 0.13
	24-36	0.12 ± 0.11	-0.33 ± 0.14	-0.08 ± 0.13
	12-24	0.13 ± 0.11	-0.35 ± 0.15	-0.15 ± 0.14
	0-12	-0.47 ± 0.13	-1.08 ± 0.18	-0.92 ± 0.17
14[c]	48-60	-0.87 ± 0.12	-2.16 ± 0.18	-1.83 ± 0.17
	36-48	0.03 ± 0.11	-0.97 ± 0.15	-0.76 ± 0.14
	24-36	0.16 ± 0.11	-0.85 ± 0.15	-0.65 ± 0.13
	12-24	0.09 ± 0.11	-0.98 ± 0.16	-0.75 ± 0.14
	0-12	-0.55 ± 0.13	-1.92 ± 0.20	-1.47 ± 0.18
22[d]	48-60	-1.22 ± 0.12	-5.11 ± 0.21	-4.60 ± 0.18
	36-48	0.04 ± 0.11	-4.02 ± 0.17	-3.58 ± 0.15
	24-36	0.14 ± 0.11	-3.85 ± 0.16	-3.47 ± 0.14
	12-24	0.07 ± 0.11	-3.85 ± 0.17	-3.62 ± 0.15
	0-12	-0.95 ± 0.13	-4.87 ± 0.22	-4.34 ± 0.20

[a] 2D Σ (cm^{-1}): 0.4539 ± 0.01%
[b] 2D Σ (cm^{-1}): 0.4546 ± 0.01%
[c] 2D Σ (cm^{-1}): 0.4553 ± 0.01%
[d] 2D Σ (cm^{-1}): 0.4484 ± 0.01%

Table 29 shows the percent error of group 2 of 8 macroscopic scattering cross sections in moderator rods #2 and #17 incurred by using 2D assembly data to approximate the drums-in core configuration.

Table 29 – Error of Macroscopic Scattering Cross Sections in Moderator Incurred by Using 2D Data to Approximate Drums-in Core Configuration, Group 2 of 8

Location		Error (% ± 1σ)		
Rod #	z (cm)	Assembly A	Assembly B	Assembly C
02[a]	48-60	-0.66 ± 0.10	-1.24 ± 0.14	-0.96 ± 0.12
	36-48	0.08 ± 0.09	-0.33 ± 0.13	-0.13 ± 0.11
	24-36	0.12 ± 0.09	-0.22 ± 0.12	-0.11 ± 0.11
	12-24	0.07 ± 0.09	-0.24 ± 0.13	-0.14 ± 0.12
	0-12	-0.52 ± 0.11	-0.96 ± 0.16	-0.78 ± 0.14
17[b]	48-60	-0.89 ± 0.10	-4.07 ± 0.20	-3.77 ± 0.18
	36-48	0.03 ± 0.09	-3.13 ± 0.17	-3.05 ± 0.15
	24-36	0.06 ± 0.09	-2.99 ± 0.16	-2.87 ± 0.15
	12-24	0.05 ± 0.10	-3.03 ± 0.18	-2.94 ± 0.16
	0-12	-0.75 ± 0.11	-3.74 ± 0.22	-3.45 ± 0.20

[a] 2D Σ (cm^{-1}): 0.8490 ± 0.01%
[b] 2D Σ (cm^{-1}): 0.8439 ± 0.01%

Table 30 shows the percent error of group 2 of 8 macroscopic scattering cross sections in moderator rods #2 and #17 incurred by using 2D assembly data to approximate the drums-out core configuration.

Table 30 – Error of Macroscopic Scattering Cross Sections in Moderator Incurred by Using 2D Data to Approximate Drums-out Core Configuration, Group 2 of 8

Location		Error (% ± 1σ)		
Rod #	z (cm)	Assembly A	Assembly B	Assembly C
02[a]	48-60	-0.75 ± 0.10	-1.11 ± 0.13	-1.00 ± 0.12
	36-48	-0.03 ± 0.10	-0.24 ± 0.12	-0.15 ± 0.11
	24-36	0.00 ± 0.09	-0.19 ± 0.12	-0.08 ± 0.10
	12-24	-0.03 ± 0.10	-0.20 ± 0.12	-0.14 ± 0.11
	0-12	-0.61 ± 0.12	-0.93 ± 0.15	-0.79 ± 0.13
17[b]	48-60	-0.93 ± 0.10	-3.36 ± 0.18	-3.04 ± 0.16
	36-48	0.00 ± 0.09	-2.52 ± 0.14	-2.27 ± 0.13
	24-36	0.04 ± 0.09	-2.42 ± 0.14	-2.21 ± 0.12
	12-24	-0.03 ± 0.10	-2.53 ± 0.15	-2.31 ± 0.13
	0-12	-0.83 ± 0.11	-3.18 ± 0.19	-2.86 ± 0.17

[a] 2D Σ (cm^{-1}): 0.8490 ± 0.01%
[b] 2D Σ (cm^{-1}): 0.8439 ± 0.01%

Table 31 shows the percent error of group 2 of 8 macroscopic scattering cross sections in heat pipes #1, #7, and #21 incurred by using 2D assembly data to approximate the drums-in core configuration.

Table 31 – Error of Macroscopic Scattering Cross Sections in Heat Pipe Incurred by Using 2D Data to Approximate Drums-in Core Configuration, Group 2 of 8

Location		Error (% ± 1σ)		
Pipe #	z (cm)	Assembly A	Assembly B	Assembly C
01[a]	48-60	-10.01 ± 0.19	-16.43 ± 0.27	-14.01 ± 0.23
	36-48	-5.94 ± 0.17	-12.32 ± 0.24	-9.58 ± 0.21
	24-36	-5.22 ± 0.17	-10.94 ± 0.24	-8.34 ± 0.21
	12-24	-5.32 ± 0.18	-11.27 ± 0.25	-8.48 ± 0.22
	0-12	-7.71 ± 0.21	-14.36 ± 0.30	-11.49 ± 0.26
07[b]	48-60	-9.41 ± 0.19	-18.47 ± 0.32	-16.65 ± 0.28
	36-48	-5.66 ± 0.17	-14.81 ± 0.28	-12.49 ± 0.25
	24-36	-4.82 ± 0.17	-13.51 ± 0.28	-11.17 ± 0.25
	12-24	-4.86 ± 0.18	-13.86 ± 0.30	-11.51 ± 0.26
	0-12	-7.25 ± 0.21	-17.18 ± 0.36	-14.75 ± 0.31
21[c]	48-60	-10.45 ± 0.19	-28.62 ± 0.42	-27.36 ± 0.38
	36-48	-6.04 ± 0.18	-25.93 ± 0.34	-24.83 ± 0.31
	24-36	-5.14 ± 0.17	-24.88 ± 0.33	-23.86 ± 0.30
	12-24	-5.22 ± 0.18	-25.14 ± 0.36	-24.31 ± 0.32
	0-12	-8.58 ± 0.22	-27.40 ± 0.45	-26.45 ± 0.41

[a] 2D Σ (cm^{-1}): 0.1376 ± 0.02%
[b] 2D Σ (cm^{-1}): 0.1346 ± 0.02%
[c] 2D Σ (cm^{-1}): 0.1254 ± 0.02%

Table 32 shows the percent error of group 2 of 8 macroscopic scattering cross sections in heat pipes #1, #7, and #21 incurred by using 2D assembly data to approximate the drums-out core configuration.

Table 32 – Error of Macroscopic Scattering Cross Sections in Heat Pipe Incurred by Using 2D Data to Approximate Drums-out Core Configuration, Group 2 of 8

Location		Error (% ± 1σ)		
Pipe #	z (cm)	Assembly A	Assembly B	Assembly C
01[a]	48-60	-11.35 ± 0.21	-15.42 ± 0.26	-13.84 ± 0.23
	36-48	-7.58 ± 0.19	-11.16 ± 0.23	-9.35 ± 0.21
	24-36	-6.59 ± 0.19	-9.76 ± 0.22	-7.90 ± 0.20
	12-24	-6.72 ± 0.20	-10.17 ± 0.24	-8.35 ± 0.22
	0-12	-9.22 ± 0.23	-13.56 ± 0.29	-11.55 ± 0.26
07[b]	48-60	-10.66 ± 0.20	-16.80 ± 0.30	-14.98 ± 0.26
	36-48	-6.54 ± 0.18	-12.55 ± 0.25	-10.56 ± 0.23
	24-36	-5.76 ± 0.18	-11.19 ± 0.25	-9.22 ± 0.22
	12-24	-5.96 ± 0.19	-12.08 ± 0.26	-9.68 ± 0.24
	0-12	-8.53 ± 0.23	-15.56 ± 0.32	-13.62 ± 0.29
21[c]	48-60	-10.77 ± 0.20	-26.40 ± 0.36	-24.96 ± 0.32
	36-48	-6.49 ± 0.18	-22.88 ± 0.29	-21.10 ± 0.26
	24-36	-5.44 ± 0.18	-21.97 ± 0.28	-19.72 ± 0.25
	12-24	-5.69 ± 0.19	-22.75 ± 0.30	-20.51 ± 0.27
	0-12	-9.06 ± 0.23	-25.68 ± 0.39	-23.92 ± 0.34

[a] 2D Σ (cm^{-1}): 0.1376 ± 0.02%
[b] 2D Σ (cm^{-1}): 0.1346 ± 0.02%
[c] 2D Σ (cm^{-1}): 0.1254 ± 0.02%

4.5.3 Macroscopic Fission Cross Sections

Table 33 shows the percent error of group 2 of 8 macroscopic fission cross sections in fuel pins #4, #8, #14, and #22 incurred by using 2D assembly data to approximate the drums-in core configuration.

Table 33 – Error of Macroscopic Fission Cross Sections in Fuel Incurred by Using 2D Data to Approximate Drums-in Core Configuration, Group 2 of 8

Location		Error (% ± 1σ)		
Pin #	z (cm)	Assembly A	Assembly B	Assembly C
04[a]	48-60	-0.49 ± 0.11	-1.21 ± 0.16	-0.88 ± 0.14
	36-48	0.19 ± 0.10	-0.23 ± 0.15	-0.07 ± 0.13
	24-36	0.22 ± 0.10	-0.17 ± 0.14	0.07 ± 0.13
	12-24	0.21 ± 0.11	-0.11 ± 0.15	0.04 ± 0.14
	0-12	-0.30 ± 0.12	-0.84 ± 0.18	-0.55 ± 0.16
08[b]	48-60	-0.48 ± 0.11	-1.59 ± 0.18	-1.21 ± 0.16
	36-48	0.23 ± 0.10	-0.55 ± 0.16	-0.34 ± 0.14
	24-36	0.23 ± 0.10	-0.35 ± 0.16	-0.17 ± 0.14
	12-24	0.26 ± 0.11	-0.49 ± 0.17	-0.17 ± 0.15
	0-12	-0.29 ± 0.12	-1.19 ± 0.20	-0.92 ± 0.18
14[c]	48-60	-0.66 ± 0.11	-2.53 ± 0.21	-2.27 ± 0.19
	36-48	0.17 ± 0.10	-1.53 ± 0.18	-1.30 ± 0.16
	24-36	0.22 ± 0.10	-1.38 ± 0.17	-1.11 ± 0.16
	12-24	0.21 ± 0.11	-1.37 ± 0.19	-1.21 ± 0.17
	0-12	-0.34 ± 0.13	-2.19 ± 0.23	-1.74 ± 0.21
22[d]	48-60	-1.00 ± 0.11	-5.82 ± 0.24	-5.69 ± 0.22
	36-48	0.08 ± 0.10	-5.01 ± 0.20	-4.85 ± 0.18
	24-36	0.13 ± 0.10	-4.76 ± 0.19	-4.63 ± 0.18
	12-24	0.08 ± 0.11	-4.94 ± 0.21	-4.77 ± 0.19
	0-12	-0.77 ± 0.13	-5.57 ± 0.26	-5.22 ± 0.24

[a] 2D Σ (cm^{-1}): 0.01064 ± 0.01%
[b] 2D Σ (cm^{-1}): 0.01065 ± 0.01%
[c] 2D Σ (cm^{-1}): 0.01066 ± 0.01%
[d] 2D Σ (cm^{-1}): 0.01047 ± 0.01%

Table 34 shows the percent error of group 2 of 8 macroscopic fission cross sections in fuel pins #4, #8, #14, and #22 incurred by using 2D assembly data to approximate the drums-out core configuration.

Table 34 – Error of Macroscopic Fission Cross Sections in Fuel Incurred by Using 2D Data to Approximate Drums-out Core Configuration, Group 2 of 8

Location		Error (% ± 1σ)		
Pin #	z (cm)	Assembly A	Assembly B	Assembly C
04[a]	48-60	-0.66 ± 0.12	-1.10 ± 0.16	-0.92 ± 0.14
	36-48	0.11 ± 0.11	-0.16 ± 0.14	-0.03 ± 0.12
	24-36	0.11 ± 0.11	-0.09 ± 0.13	0.00 ± 0.12
	12-24	0.13 ± 0.11	-0.14 ± 0.14	0.00 ± 0.13
	0-12	-0.41 ± 0.13	-0.80 ± 0.17	-0.62 ± 0.16
08[b]	48-60	-0.72 ± 0.12	-1.40 ± 0.17	-1.02 ± 0.15
	36-48	0.08 ± 0.11	-0.41 ± 0.15	-0.15 ± 0.13
	24-36	0.11 ± 0.11	-0.29 ± 0.14	-0.08 ± 0.13
	12-24	0.10 ± 0.11	-0.32 ± 0.15	-0.14 ± 0.14
	0-12	-0.41 ± 0.13	-0.95 ± 0.18	-0.83 ± 0.17
14[c]	48-60	-0.80 ± 0.12	-1.95 ± 0.19	-1.66 ± 0.17
	36-48	0.01 ± 0.11	-0.91 ± 0.15	-0.75 ± 0.14
	24-36	0.12 ± 0.11	-0.84 ± 0.15	-0.66 ± 0.13
	12-24	0.07 ± 0.11	-0.97 ± 0.16	-0.77 ± 0.14
	0-12	-0.51 ± 0.13	-1.76 ± 0.20	-1.39 ± 0.18
22[d]	48-60	-1.13 ± 0.12	-4.78 ± 0.21	-4.34 ± 0.18
	36-48	0.05 ± 0.11	-3.87 ± 0.17	-3.49 ± 0.15
	24-36	0.09 ± 0.11	-3.71 ± 0.16	-3.38 ± 0.14
	12-24	0.03 ± 0.11	-3.71 ± 0.17	-3.51 ± 0.15
	0-12	-0.92 ± 0.13	-4.52 ± 0.22	-4.10 ± 0.20

[a] 2D Σ (cm^{-1}): 0.01064 ± 0.01%
[b] 2D Σ (cm^{-1}): 0.01065 ± 0.01%
[c] 2D Σ (cm^{-1}): 0.01066 ± 0.01%
[d] 2D Σ (cm^{-1}): 0.01047 ± 0.01%

4.5.4 Discussion

Two key trends can be seen from the data in the preceding tables, both of which arise from the thermalizing effect of neighboring beryllium reflector. The first arises in the two axial regions – $z = 0 - 12$ cm and $z = 48 - 60$ cm – closest to the axial reflectors: in no case in any fuel pin, moderator rod, or heat pipe does a core cross section equal its 2D single assembly approximation. The second arises in peripheral fuel pins and moderator rods in Assemblies B and C: such elements are radially close enough to beryllium Blocks that thermalization statistically invalidates the use of approximation by data describing the 2D single assembly. Core cross sections that can be well approximated by use of the 2D single assembly data are almost always in the center three axial regions and either in Assembly A or closer to the center of a fuel assembly than its periphery. While some such cross sections skirt the limits of statistical significance, this rule of thumb holds for fuel pins and moderator rods regardless of drum rotation. Rotating the drums outward reduces these discrepancies, but not enough to create statistical negligence. No heat pipe core cross section matches its 2D assembly counterpart.

4.6 Comparison of 3D Single Assembly Data against 2D Single Assembly Data

This section investigates environmental effects in core configurations via comparison of regionwide cross sections between 3D assembly configurations against those generated by analysis of the 2D single assembly. These single assembly configurations exaggerate certain properties of the core such as the number of fuel assemblies (3D mixed), the thickness of the reflector (3D specular), or the leakage of the system (3D vacuum). Thus, these configurations are expected to produce different sets of environmental effects for further analysis.

The tables in this section contain macroscopic data in energy Group 2 of 8 – between 5.53 and 821 keV) – of the selected regions of elements in the 2D single assembly problem. This energy group was chosen as the contrast between cross sections generated for the 3D assemblies and those for the 2D single assembly was the greatest in this group for prevailing reactions within each material. Each region is paired with the three data of the corresponding region within each 3D single assembly configuration, written as percents error incurred by using the 2D single assembly data to approximate the true 3D assembly data.

4.6.1 Macroscopic Capture Cross Sections

Table 35 shows the percent error of group 2 of 8 macroscopic capture cross sections in fuel pins #4, #8, #14, and #22 incurred by using 2D assembly data to approximate the 3D assembly configurations.

Table 35 – Error of Macroscopic Capture Cross Sections in Fuel Incurred by Using 2D Data to Approximate 3D Assembly Configurations, Group 2 of 8

Location		Error (% ± 1σ)		
Pin #	z (cm)	3D Specular	3D Mixed	3D Vacuum
04[a]	48-60	-0.47 ± 0.04	-0.68 ± 0.03	4.70 ± 0.04
	36-48	-0.04 ± 0.04	0.32 ± 0.03	5.63 ± 0.03
	24-36	-0.03 ± 0.03	0.33 ± 0.03	5.59 ± 0.03
	12-24	-0.04 ± 0.03	0.32 ± 0.03	5.60 ± 0.03
	0-12	-0.38 ± 0.03	-0.44 ± 0.04	4.80 ± 0.04
08[b]	48-60	-0.50 ± 0.04	-0.70 ± 0.03	4.85 ± 0.04
	36-48	-0.04 ± 0.04	0.33 ± 0.03	5.74 ± 0.04
	24-36	-0.02 ± 0.03	0.35 ± 0.03	5.74 ± 0.03
	12-24	-0.04 ± 0.03	0.34 ± 0.03	5.75 ± 0.04
	0-12	-0.41 ± 0.03	-0.46 ± 0.04	4.95 ± 0.04
14[c]	48-60	-0.63 ± 0.04	-0.86 ± 0.03	5.10 ± 0.05
	36-48	-0.04 ± 0.03	0.32 ± 0.03	6.00 ± 0.04
	24-36	-0.05 ± 0.03	0.32 ± 0.03	6.04 ± 0.04
	12-24	-0.07 ± 0.03	0.32 ± 0.03	6.02 ± 0.04
	0-12	-0.51 ± 0.03	-0.57 ± 0.04	5.18 ± 0.05
22[d]	48-60	-1.40 ± 0.04	-1.50 ± 0.04	4.72 ± 0.07
	36-48	-0.11 ± 0.04	0.24 ± 0.03	5.67 ± 0.06
	24-36	-0.06 ± 0.04	0.30 ± 0.03	5.63 ± 0.06
	12-24	-0.09 ± 0.03	0.25 ± 0.04	5.60 ± 0.06
	0-12	-1.20 ± 0.03	-1.31 ± 0.04	4.70 ± 0.08

[a] 2D Σ (cm^{-1}): 0.009505 ± 0.01%
[b] 2D Σ (cm^{-1}): 0.009518 ± 0.01%
[c] 2D Σ (cm^{-1}): 0.009520 ± 0.01%
[d] 2D Σ (cm^{-1}): 0.009184 ± 0.01%

4.6.2 Macroscopic Scattering Cross Sections

Table 36 shows the percent error of group 2 of 8 macroscopic scattering cross sections in fuel pins #4, #8, #14, and #22 incurred by using 2D assembly data to approximate the 3D assembly configurations.

Table 36 – Error of Macroscopic Scattering Cross Sections in Fuel Incurred by Using 2D Data to Approximate 3D Assembly Configurations, Group 2 of 8

Location		Error (% ± 1σ)		
Pin #	z (cm)	3D Specular	3D Mixed	3D Vacuum
04[a]	48-60	-0.32 ± 0.03	-0.46 ± 0.03	2.86 ± 0.03
	36-48	-0.02 ± 0.03	0.21 ± 0.03	3.48 ± 0.03
	24-36	-0.02 ± 0.03	0.21 ± 0.03	3.48 ± 0.03
	12-24	-0.03 ± 0.03	0.20 ± 0.03	3.48 ± 0.03
	0-12	-0.29 ± 0.03	-0.30 ± 0.04	2.93 ± 0.04
08[b]	48-60	-0.34 ± 0.03	-0.48 ± 0.03	2.95 ± 0.04
	36-48	-0.03 ± 0.03	0.21 ± 0.03	3.58 ± 0.03
	24-36	-0.01 ± 0.03	0.22 ± 0.03	3.59 ± 0.03
	12-24	-0.02 ± 0.03	0.22 ± 0.03	3.59 ± 0.03
	0-12	-0.30 ± 0.03	-0.32 ± 0.04	3.00 ± 0.04
14[c]	48-60	-0.40 ± 0.03	-0.57 ± 0.03	3.21 ± 0.05
	36-48	-0.03 ± 0.03	0.19 ± 0.03	3.84 ± 0.04
	24-36	-0.03 ± 0.03	0.21 ± 0.03	3.86 ± 0.04
	12-24	-0.04 ± 0.03	0.20 ± 0.03	3.85 ± 0.04
	0-12	-0.35 ± 0.03	-0.37 ± 0.04	3.25 ± 0.05
22[d]	48-60	-0.81 ± 0.03	-0.96 ± 0.03	3.48 ± 0.07
	36-48	-0.06 ± 0.03	0.15 ± 0.03	4.13 ± 0.06
	24-36	-0.04 ± 0.03	0.20 ± 0.03	4.13 ± 0.06
	12-24	-0.05 ± 0.03	0.16 ± 0.03	4.11 ± 0.06
	0-12	-0.73 ± 0.03	-0.79 ± 0.04	3.47 ± 0.07

[a] 2D Σ (cm^{-1}): 0.4539 ± 0.01%
[b] 2D Σ (cm^{-1}): 0.4546 ± 0.01%
[c] 2D Σ (cm^{-1}): 0.4553 ± 0.01%
[d] 2D Σ (cm^{-1}): 0.4484 ± 0.01%

Table 37 shows the percent error of group 2 of 8 macroscopic scattering cross sections in moderator rods #2 and #17 incurred by using 2D assembly data to approximate the 3D assembly configurations.

Table 37 – Error of Macroscopic Scattering Cross Sections in Moderator Incurred by Using 2D Data to Approximate 3D Assembly Configurations, Group 2 of 8

Location		Error (% ± 1σ)		
Rod #	z (cm)	3D Specular	3D Mixed	3D Vacuum
02[a]	48-60	-0.53 ± 0.03	-0.53 ± 0.03	1.13 ± 0.03
	36-48	-0.02 ± 0.03	0.11 ± 0.03	1.70 ± 0.03
	24-36	-0.02 ± 0.03	0.11 ± 0.03	1.70 ± 0.03
	12-24	-0.02 ± 0.03	0.10 ± 0.03	1.70 ± 0.03
	0-12	-0.48 ± 0.03	-0.46 ± 0.03	1.16 ± 0.03
17[b]	48-60	-0.73 ± 0.03	-0.72 ± 0.03	1.45 ± 0.05
	36-48	-0.04 ± 0.03	0.09 ± 0.03	2.02 ± 0.04
	24-36	-0.03 ± 0.03	0.12 ± 0.03	2.01 ± 0.04
	12-24	-0.04 ± 0.03	0.09 ± 0.03	2.01 ± 0.04
	0-12	-0.66 ± 0.03	-0.66 ± 0.03	1.44 ± 0.05

[a] 2D Σ (cm^{-1}): 0.8490 ± 0.01%
[b] 2D Σ (cm^{-1}): 0.8439 ± 0.01%

Table 38 shows the percent error of group 2 of 8 macroscopic scattering cross sections in heat pipes #1, #7, and #21 incurred by using 2D assembly data to approximate the 3D assembly configurations.

Table 38 – Error of Macroscopic Scattering Cross Sections in Heat Pipe Incurred by Using 2D Data to Approximate 3D Assembly Configurations, Group 2 of 8

Location		Error (% ± 1σ)		
Pipe #	z (cm)	3D Specular	3D Mixed	3D Vacuum
01[a]	48-60	-1.41 ± 0.05	-1.16 ± 0.05	0.64 ± 0.05
	36-48	-0.09 ± 0.05	0.03 ± 0.05	1.65 ± 0.05
	24-36	-0.07 ± 0.05	0.03 ± 0.05	1.65 ± 0.05
	12-24	-0.13 ± 0.05	0.01 ± 0.05	1.65 ± 0.05
	0-12	-1.28 ± 0.05	-1.19 ± 0.06	0.63 ± 0.06
07[b]	48-60	-1.42 ± 0.05	-1.21 ± 0.05	1.52 ± 0.06
	36-48	-0.13 ± 0.05	0.05 ± 0.05	2.61 ± 0.05
	24-36	-0.11 ± 0.05	0.07 ± 0.05	2.60 ± 0.05
	12-24	-0.09 ± 0.05	0.05 ± 0.05	2.59 ± 0.05
	0-12	-1.34 ± 0.05	-1.25 ± 0.06	1.50 ± 0.06
21[c]	48-60	-2.63 ± 0.05	-2.09 ± 0.05	-0.42 ± 0.13
	36-48	-0.18 ± 0.05	-0.07 ± 0.05	0.72 ± 0.11
	24-36	-0.11 ± 0.05	-0.01 ± 0.05	0.81 ± 0.10
	12-24	-0.13 ± 0.05	-0.07 ± 0.05	0.77 ± 0.11
	0-12	-2.33 ± 0.05	-2.27 ± 0.06	-0.47 ± 0.13

[a] 2D Σ (cm^{-1}): 0.1376 ± 0.02%
[b] 2D Σ (cm^{-1}): 0.1346 ± 0.02%
[c] 2D Σ (cm^{-1}): 0.1254 ± 0.02%

4.6.3 Macroscopic Fission Cross Sections

Table 39 shows the percent error of group 2 of 8 macroscopic fission cross sections in fuel pins #4, #8, #14, and #22 incurred by using 2D assembly data to approximate the 3D assembly configurations.

Table 39 – Error of Macroscopic Fission Cross Sections in Fuel Incurred by Using 2D Data to Approximate 3D Assembly Configurations, Group 2 of 8

Location		Error (% ± 1σ)		
Pin #	z (cm)	3D Specular	3D Mixed	3D Vacuum
04[a]	48-60	-0.28 ± 0.03	-0.40 ± 0.03	2.59 ± 0.03
	36-48	-0.02 ± 0.03	0.19 ± 0.03	3.12 ± 0.03
	24-36	-0.02 ± 0.03	0.19 ± 0.03	3.11 ± 0.03
	12-24	-0.02 ± 0.03	0.18 ± 0.03	3.11 ± 0.03
	0-12	-0.24 ± 0.03	-0.26 ± 0.04	2.65 ± 0.04
08[b]	48-60	-0.30 ± 0.03	-0.42 ± 0.03	2.67 ± 0.04
	36-48	-0.02 ± 0.03	0.19 ± 0.03	3.19 ± 0.03
	24-36	-0.01 ± 0.03	0.20 ± 0.03	3.20 ± 0.03
	12-24	-0.02 ± 0.03	0.19 ± 0.03	3.20 ± 0.03
	0-12	-0.27 ± 0.03	-0.29 ± 0.04	2.72 ± 0.04
14[c]	48-60	-0.38 ± 0.03	-0.51 ± 0.03	2.83 ± 0.05
	36-48	-0.03 ± 0.03	0.18 ± 0.03	3.35 ± 0.04
	24-36	-0.02 ± 0.03	0.19 ± 0.03	3.37 ± 0.04
	12-24	-0.04 ± 0.03	0.18 ± 0.03	3.36 ± 0.04
	0-12	-0.31 ± 0.03	-0.34 ± 0.04	2.87 ± 0.05
22[d]	48-60	-0.80 ± 0.03	-0.87 ± 0.03	2.74 ± 0.07
	36-48	-0.07 ± 0.03	0.13 ± 0.03	3.28 ± 0.06
	24-36	-0.04 ± 0.03	0.17 ± 0.03	3.27 ± 0.06
	12-24	-0.05 ± 0.03	0.13 ± 0.03	3.25 ± 0.06
	0-12	-0.69 ± 0.03	-0.75 ± 0.04	2.74 ± 0.07

[a] 2D Σ (cm^{-1}): 0.01064 ± 0.01%
[b] 2D Σ (cm^{-1}): 0.01065 ± 0.01%
[c] 2D Σ (cm^{-1}): 0.01066 ± 0.01%
[d] 2D Σ (cm^{-1}): 0.01047 ± 0.01%

4.6.4 Macroscopic Nubars

Table 40 shows the percent error of group 2 of 8 macroscopic fission cross sections in fuel pins #4, #8, #14, and #22 incurred by using 2D assembly data to approximate the 3D assembly configurations.

Table 40 – Error of Macroscopic Nubars in Fuel Incurred by Using 2D Data to Approximate 3D Assembly Configurations, Group 2 of 8

Location		Error (% ± 1σ)		
Pin #	z (cm)	3D Specular	3D Mixed	3D Vacuum
04[a]	48-60	0.01 ± 0.03	0.02 ± 0.03	-0.10 ± 0.03
	36-48	0.00 ± 0.03	-0.01 ± 0.03	-0.13 ± 0.03
	24-36	0.00 ± 0.03	-0.01 ± 0.03	-0.13 ± 0.03
	12-24	0.00 ± 0.03	-0.01 ± 0.03	-0.13 ± 0.03
	0-12	0.01 ± 0.03	0.01 ± 0.03	-0.11 ± 0.03
08[b]	48-60	0.01 ± 0.03	0.02 ± 0.03	-0.11 ± 0.04
	36-48	0.00 ± 0.03	-0.01 ± 0.03	-0.13 ± 0.03
	24-36	0.00 ± 0.03	-0.01 ± 0.03	-0.13 ± 0.03
	12-24	0.00 ± 0.03	-0.01 ± 0.03	-0.13 ± 0.03
	0-12	0.01 ± 0.03	0.01 ± 0.03	-0.11 ± 0.04
14[c]	48-60	0.01 ± 0.03	0.02 ± 0.03	-0.12 ± 0.04
	36-48	0.00 ± 0.03	-0.01 ± 0.03	-0.14 ± 0.04
	24-36	0.00 ± 0.03	-0.01 ± 0.03	-0.14 ± 0.04
	12-24	0.00 ± 0.03	-0.01 ± 0.03	-0.14 ± 0.04
	0-12	0.01 ± 0.03	0.01 ± 0.03	-0.12 ± 0.05
22[d]	48-60	0.03 ± 0.03	0.03 ± 0.03	-0.13 ± 0.07
	36-48	0.00 ± 0.03	-0.01 ± 0.03	-0.15 ± 0.06
	24-36	0.00 ± 0.03	-0.01 ± 0.03	-0.15 ± 0.05
	12-24	0.00 ± 0.03	-0.01 ± 0.03	-0.15 ± 0.06
	0-12	0.03 ± 0.03	0.03 ± 0.04	-0.13 ± 0.07

[a] 2D ν: 2.450 ± 0.01%
[b] 2D ν: 2.450 ± 0.01%
[c] 2D ν: 2.449 ± 0.01%
[d] 2D ν: 2.451 ± 0.01%

4.6.5 Discussion

As seen in the tables in the previous section, cross sections of the capture, scattering and fission reactions all follow similar trends in all materials. Returning the axial reflectors back to the 2D specular assembly creates the 3D specular assembly. These reflectors then reflect thermalized neutrons back into the core, softening the flux at the top and bottom. As neutron energy decreases, cross sections generally increase in this energy group as evident near the axial periphery of the assembly. From the 3D specular assembly, removing the axial specular boundary condition creates the 3D mixed assembly problem, slightly increasing axial leakage. Cross sections significantly increase at the center and decrease near the top and bottom due to fast leakage through the reflectors. Removing all specular boundary conditions creates the 3D vacuum assembly problem. Leakage drastically increases, hardening the flux and significantly increasing cross sections throughout the assembly, especially at peripheral regions.

The trends for cross sections do not apply to nubar, which is a weak function of energy in this group. No significant function of boundary condition or position within the assembly is observed.

CHAPTER 5. FUTURE WORK

As stated previously, subsequent work has been proposed in modeling the design presented in this thesis using a plausible temperature profile for the materials in the fuel assembly – that is, the fuel being hotter than the moderator. In addition, given the fission rate distributions provided, this design can be analyzed via thermal hydraulic methods to generate a more realistic temperature distribution at the expense of higher computational cost to process the temperature data in the neutronics stage where benchmark results are generated. The core configuration can also be developed further to yield improvements such as lowering the controlled reactivity at beginning of cycle, increasing control drum worth, and ensuring the presence of a negative temperature coefficient of reactivity throughout the range of possible operating temperatures.

In addition, flux spectra can be tallied in a regionwide basis to confirm or deny the assertations that a given shifting of this spectrum is responsible for a change in cross sections as a function of location. These tallies should be accompanied by an analysis of isotopic cross sections, as the presence of resonances jeopardizes any rule of thumb that can be made describing these values.

An investigation of the heat pipe isotopes for resonances is also merited to determine its exaggerated response to position on its cross sections as compared to fuel rods and heat pipes.

APPENDIX A. SUMMARY OF ATTACHED FILES

Attached to this thesis are SERPENT 2[4] input files for each benchmark problem discussed as well as their respective output files, as well as tables containing the complete sets of 2-, 4-, and 8-group multigroup data and scattering kernel. These data are made available in raw format and human-readable tables for utility and ease of use. Below is a description of the attached files and how they are read to obtain the results presented.

A.1 Multigroup Cross Section and Nubar Files

The input and output files that calculate and contain multigroup data, including cross sections and nubar, are in the `serpent` directory of the file `MSThesisSommer2022.zip`. The naming conventions and structure of these files are discussed in this section.

A.1.1 File Naming Format

Each filename is composed of a prefix and a suffix. The prefix of a filename denotes what benchmark problem the named file is describing and is one of the following:

- `casezero` – 2D single assembly (case upon which other sets are compared)
- `arsas` – 3D specular assembly (Assembly, Radial Specular, Axial Specular)
- `arsav` – 3D mixed assembly (Assembly, Radial Specular, Axial Vacuum)
- `arvav` – 3D vacuum assembly (Assembly, Radial Vacuum, Axial Vacuum)
- `drumsin2` – Full core configuration, DRUMS rotated INward
- `drumsout2` – Full core configuration with DRUMS rotated OUTward

Each benchmark problem has eight files, each of which having a suffix detailing its purpose. The list of suffixes and their respective definitions are as listed:

- `.pbs` – Portable Batch Script file, configured to run SERPENT 2[4] on the INL Sawtooth cluster.
- `.sss` – SERPENT 2[4] input file. Discussed further in Section A.1.2.
- `.sss.out` – Nuclear and material data. Not used in thesis.
- `.sss.seed` – Randum number generator seed used for last run. Not used in thesis.
- `.sss.stdout` – File to which standard output is piped. Not used in thesis.
- `.sss_arr0.m` – Reaction rate output file. Not used in thesis.
- `.sss_det0.m` – Detector output file. Discussed further in Section A.1.4.
- `.sss_res.m` – Main output file. Discussed further in Section A.1.3.

A.1.2 Input File Structure

An example input file for the 2D single assembly is included in Appendix B. The input file defines cells, surfaces, and material compositions as written in CHAPTER 2. Multigroup data are output via the use of detector cards which are named based on the type of output. The list of possible names are as follows:

- `flSPP` – flux in pin index `PP` in assembly `S`
- `flS` – flux averaged in block `S`
- `ffS` – fuel flux averaged in assembly `S`
- `fmS` – moderator flux averaged in assembly `S`

- `RRRSPP` – macroscopic cross section of reaction `RRR` (listed below) in pin `PP` in assembly `S`
  - `txs` – total
  - `cxs` – capture
  - `sxs` – scattering
  - `fxs` – fission
  - `nb` – nubar
  - `nxn` – (n, xn)
- `RRRS` – macroscopic cross section of reaction RRR in block S
- `RRRSPPXAAA` – microscopic cross section of reaction `RRR` in pin `PP` in assembly `S` of isotope `X-AAA`.
- `RRRSXAAA` – microscopic cross section of reaction `RRR` in block `S`

In input files involving a single assembly, the assembly designator in detector names is omitted to represent the output of that detector throughout the assembly.

A.1.3 Main Output File Structure

The main output file `*.sss_res.m` contains, among other outputs, two calculated sets of values used for results in this thesis. They are:

- `IMP_KEFF` – implicit estimate of eigenvalue along with its relative 1σ.
- `B1_SN` – interleaved `N`th Legendre moment of scattering kernel and relative 1σ for each value. The odd-indexed values that compose the Legendre moment can be written row-by-row to retrieve the matrix itself, and the even-index values denote

the relative 1σ for each value in the Legendre moment. The Legendre moment is a *G*-by-*G* matrix (with *G* being number of energy groups), where the element in the *i*th row and *j*th column contains the scattering cross section from energy group *i* to *j*. Input files not in a subdirectory (`g2`, `g4`, or `g8`) will not have the input card that activates scattering kernel calculation and corresponding output files will have all zeros for this value. Input files in a subdirectory calculate scattering kernels denoted by the subdirectory name and are further discussed in Section A.2.

A.1.4 Detector Output File Structure

The detector output file `*.sss_det0.m` contains the outputs for all detectors in the respective input file. Each detector has its data bounded in square brackets with each line of the following format:

```
VAL EBIN 1 1 1 1 1 ZBIN 1 1 MEAN_VAL RSU
```

- `VAL` – index of value
- `EBIN` – current energy group bin
- `ZBIN` – current axial position bin
    - 1 for $z = 0 - 12$ cm, 2 for $z = 12 - 24$ cm, etc. for pins/rods/pipes
    - 1 otherwise
- `MEAN_VAL` – mean value of statistic
- `RSU` – 1σ of statistic

A.2 Multigroup Scattering Kernel Files

The input and output files that calculate and contain multigroup Legendre moments of the scattering kernel are in the `g2`, `g4`, or `g8` subdirectory of `serpent`, with the number after `g` denoting the number of energy groups for which the moments are calculated. Scattering kernel data presented in this thesis are retrieved from the main output files in these subdirectories. In the case of full core configuration benchmark problems, the main output file contains three sets of outputs – the first for Assembly A, the second for Assembly B, and the third for Assembly C.

A.3. Multigroup Data Tables

Included in the `tables` directory of the file `MSThesisSommer2022.zip` are four word documents containing macroscopic (cm^{-1}) and microscopic (b) cross sections, nubars, and scattering kernels, along with their respective relative statistical uncertainties for all benchmark problems, selected regions, and isotopes in fuel, moderator, reflector, and absorber. These tables are post processed from the SERPENT 2[4] output files discussed above and are named as follows:

- `2-Group.docx` – Complete set of two-group cross sections and nubars.
- `4-Group.docx` – Complete set of four-group cross sections and nubars.
- `8-Group.docx` – Complete set of eight-group cross sections and nubars.
- `Scattering Kernel Data.docx` – Assembly-averaged 2-, 4-, and 8-group Legendre moments of the scattering kernel up to seventh degree.

APPENDIX B. EXAMPLE SERPENT 2 INPUT FILE

The following text is the SERPENT 2[4] input file used for the 2D single assembly benchmark problem. The code with additional comments is included in this appendix to facilitate the replication of the presented results using an arbitrary continuous energy code.

```
set title "Case 0: Full Length Single Assembly, 2D"
%**************************CELLS*****************************
% ---Assembly Lattice---
lat 9 2 0 0 19 19 2.15
      3 3 3 3 3 3 3 3 3 3 3 3 3 3 3 3 3 3 3
       3 3 3 3 3 3 3 3 3 6 4 6 4 6 4 6 4 6 3
        3 3 3 3 3 3 3 3 4 5 5 5 5 5 5 5 5 4 3
         3 3 3 3 3 3 3 6 5 6 4 6 4 6 4 6 5 6 3
          3 3 3 3 3 3 4 5 4 5 5 5 5 5 5 4 5 4 3
           3 3 3 3 3 6 5 6 5 6 4 6 4 6 5 6 5 6 3
            3 3 3 3 4 5 4 5 4 5 5 5 5 4 5 4 5 4 3
             3 3 3 6 5 6 5 6 5 6 4 6 5 6 5 6 5 6 3
              3 3 4 5 4 5 4 5 4 5 5 4 5 4 5 4 5 4 3
               3 6 5 6 5 6 5 6 5 6 5 6 5 6 5 6 5 6 3
                3 4 5 4 5 4 5 4 5 5 4 5 4 5 4 5 4 3 3
                 3 6 5 6 5 6 5 6 4 6 5 6 5 6 5 6 3 3 3
                  3 4 5 4 5 4 5 5 5 5 4 5 4 5 4 3 3 3 3
                   3 6 5 6 5 6 4 6 4 6 5 6 5 6 3 3 3 3 3
                    3 4 5 4 5 5 5 5 5 5 4 5 4 3 3 3 3 3 3
                     3 6 5 6 4 6 4 6 4 6 5 6 3 3 3 3 3 3 3
                      3 4 5 5 5 5 5 5 5 5 4 3 3 3 3 3 3 3 3
                       3 6 4 6 4 6 4 6 4 6 3 3 3 3 3 3 3 3 3
                        3 3 3 3 3 3 3 3 3 3 3 3 3 3 3 3 3 3 3
% ---Assembly---
cell 200 0    void      10 -99       % assembly gap
cell 202 0    fill 9    -10          % assembly lattice window
% ---Monolith---
cell 301 3    monolith  -inf         % monolith
% ---Fuel---
cell 401 4    fuel      -41          % fuel
cell 402 4    void      41 -42       % gap
cell 403 4    monolith  42 -inf      % monolith
% ---Moderator---
cell 501 5    moderator -51          % moderator
cell 502 5    void      51 -52       % gap
cell 503 5    monolith  52 -inf      % monolith
% ---Heat Pipe---
cell 601 6    htpipe    -60          % heat pipe
cell 602 6    monolith   60 -inf     % monolith
```

```
% ---Outside---
cell 998 0    void      20 -99       % limbo
cell 999 0    outside   99           % graveyard
%*************************SURFACES*************************
surf 10 hexyprism 0 0 16.0765 0 60   % assembly without reflector
surf 41 cyl 0 0 0.925                % fuel radius
surf 42 cyl 0 0 0.975                % fuel gap
surf 51 cyl 0 0 0.95                 % moderator radius
surf 52 cyl 0 0 1                    % moderator gap
surf 60 cyl 0 0 1                    % heat pipe radius
surf 99 hexyprism 0 0 16.2765 0 60   % viewing window
surf inf inf
%***************************DATA***************************
set acelib "/home/sommar/SERPENT/xsdata/endf80.xsdata"
set pop 1000000 10000 1000           % KCODE 100000 1 110 10
set bc 2                             % specular bc
set power 2.0e6                      % assume 2 MWth
set arr 2                            % output reaction rates
% ---Energy Grid---
ene 1 4 scale238                     % flux spectrum bins
ene 2 4 cas8                         % 8-group bins
% ---Detector Cells---
surf 200 cyl 0 0 20 0 60
cell d04 -04 void -41 -10 -200 trans U -04 3.225 1.861954618 0
cell d08 -08 void -41 -10 -200 trans U -08 5.375 5.585863854 0
cell d14 -14 void -41 -10 -200 trans U -14 7.525 9.309773091 0
cell d22 -22 void -41 -10 -200 trans U -22 9.675 13.03368223 0
cell d02 -02 void -51 -10 -200 trans U -02 1.075 1.861954618 0
cell d17 -17 void -51 -10 -200 trans U -17 7.525 13.03368233 0
cell d01 -01 void -60 -10 -200 trans U -01 0 0 0
cell d07 -07 void -60 -10 -200 trans U -07 4.3 7.447818473 0
cell d21 -21 void -60 -10 -200 trans U -21 8.6 14.89563695 0
% ---Flux---
det fl04 du -04 de 2
det fl08 du -08 de 2
det fl14 du -14 de 2
det fl22 du -22 de 2
det fl02 du -02 de 2
det fl17 du -17 de 2
det fl01 du -01 de 2
det fl07 du -07 de 2
det fl21 du -21 de 2
% ---Material Flux---
det ff dm fuel      de 1 dt -3
det fm dm moderator de 1 dt -3
% ---Macro Total---
det txs04 du -04 de 2 dr -1 fuel      dt 3 fl04
det txs08 du -08 de 2 dr -1 fuel      dt 3 fl08
det txs14 du -14 de 2 dr -1 fuel      dt 3 fl14
det txs22 du -22 de 2 dr -1 fuel      dt 3 fl22
det txs02 du -02 de 2 dr -1 moderator dt 3 fl02
det txs17 du -17 de 2 dr -1 moderator dt 3 fl17
```

```
det txs01 du -01 de 2 dr -1 htpipe    dt 3 fl01
det txs07 du -07 de 2 dr -1 htpipe    dt 3 fl07
det txs21 du -21 de 2 dr -1 htpipe    dt 3 fl21
% ---Macro Capture---
det cxs04 du -04 de 2 dr -2 fuel      dt 3 fl04
det cxs08 du -08 de 2 dr -2 fuel      dt 3 fl08
det cxs14 du -14 de 2 dr -2 fuel      dt 3 fl14
det cxs22 du -22 de 2 dr -2 fuel      dt 3 fl22
det cxs02 du -02 de 2 dr -2 moderator dt 3 fl02
det cxs17 du -17 de 2 dr -2 moderator dt 3 fl17
det cxs01 du -01 de 2 dr -2 htpipe    dt 3 fl01
det cxs07 du -07 de 2 dr -2 htpipe    dt 3 fl07
det cxs21 du -21 de 2 dr -2 htpipe    dt 3 fl21
% ---Macro Scattering---
det sxs04 du -04 de 2 dr -3 fuel      dt 3 fl04
det sxs08 du -08 de 2 dr -3 fuel      dt 3 fl08
det sxs14 du -14 de 2 dr -3 fuel      dt 3 fl14
det sxs22 du -22 de 2 dr -3 fuel      dt 3 fl22
det sxs02 du -02 de 2 dr -3 moderator dt 3 fl02
det sxs17 du -17 de 2 dr -3 moderator dt 3 fl17
det sxs01 du -01 de 2 dr -3 htpipe    dt 3 fl01
det sxs07 du -07 de 2 dr -3 htpipe    dt 3 fl07
det sxs21 du -21 de 2 dr -3 htpipe    dt 3 fl21
% ---Macro Fission---
det fxs04 du -04 de 2 dr -6 fuel      dt 3 fl04
det fxs08 du -08 de 2 dr -6 fuel      dt 3 fl08
det fxs14 du -14 de 2 dr -6 fuel      dt 3 fl14
det fxs22 du -22 de 2 dr -6 fuel      dt 3 fl22
% ---Macro Nubar---
det nb04 du -04 de 2 dr -7 fuel       dt 3 fxs04
det nb08 du -08 de 2 dr -7 fuel       dt 3 fxs08
det nb14 du -14 de 2 dr -7 fuel       dt 3 fxs14
det nb22 du -22 de 2 dr -7 fuel       dt 3 fxs22
% ---Macro (n, xn)---
det nxn04 du -04 de 2 dr -16 fuel      dt 3 fl04
det nxn08 du -08 de 2 dr -16 fuel      dt 3 fl08
det nxn14 du -14 de 2 dr -16 fuel      dt 3 fl14
det nxn22 du -22 de 2 dr -16 fuel      dt 3 fl22
det nxn02 du -02 de 2 dr -16 moderator dt 3 fl02
det nxn17 du -17 de 2 dr -16 moderator dt 3 fl17
det nxn01 du -01 de 2 dr -16 htpipe    dt 3 fl01
det nxn07 du -07 de 2 dr -16 htpipe    dt 3 fl07
det nxn21 du -21 de 2 dr -16 htpipe    dt 3 fl21
% ---Micro Total---
det txs04n14  du -04 de 2 dr -1 n14  dt 3 fl04
det txs08n14  du -08 de 2 dr -1 n14  dt 3 fl08
det txs14n14  du -14 de 2 dr -1 n14  dt 3 fl14
det txs22n14  du -22 de 2 dr -1 n14  dt 3 fl22
det txs04n15  du -04 de 2 dr -1 n15  dt 3 fl04
det txs08n15  du -08 de 2 dr -1 n15  dt 3 fl08
det txs14n15  du -14 de 2 dr -1 n15  dt 3 fl14
det txs22n15  du -22 de 2 dr -1 n15  dt 3 fl22
```

```
det txs04u235 du -04 de 2 dr -1 u235 dt 3 fl04
det txs08u235 du -08 de 2 dr -1 u235 dt 3 fl08
det txs14u235 du -14 de 2 dr -1 u235 dt 3 fl14
det txs22u235 du -22 de 2 dr -1 u235 dt 3 fl22
det txs04u238 du -04 de 2 dr -1 u238 dt 3 fl04
det txs08u238 du -08 de 2 dr -1 u238 dt 3 fl08
det txs14u238 du -14 de 2 dr -1 u238 dt 3 fl14
det txs22u238 du -22 de 2 dr -1 u238 dt 3 fl22
det txs02h1   du -02 de 2 dr -1 h1   dt 3 fl02
det txs17h1   du -17 de 2 dr -1 h1   dt 3 fl17
det txs02y89  du -02 de 2 dr -1 y89  dt 3 fl02
det txs17y89  du -17 de 2 dr -1 y89  dt 3 fl17
% ---Micro Capture---
det cxs04n14  du -04 de 2 dr -2 n14  dt 3 fl04
det cxs08n14  du -08 de 2 dr -2 n14  dt 3 fl08
det cxs14n14  du -14 de 2 dr -2 n14  dt 3 fl14
det cxs22n14  du -22 de 2 dr -2 n14  dt 3 fl22
det cxs04n15  du -04 de 2 dr -2 n15  dt 3 fl04
det cxs08n15  du -08 de 2 dr -2 n15  dt 3 fl08
det cxs14n15  du -14 de 2 dr -2 n15  dt 3 fl14
det cxs22n15  du -22 de 2 dr -2 n15  dt 3 fl22
det cxs04u235 du -04 de 2 dr -2 u235 dt 3 fl04
det cxs08u235 du -08 de 2 dr -2 u235 dt 3 fl08
det cxs14u235 du -14 de 2 dr -2 u235 dt 3 fl14
det cxs22u235 du -22 de 2 dr -2 u235 dt 3 fl22
det cxs04u238 du -04 de 2 dr -2 u238 dt 3 fl04
det cxs08u238 du -08 de 2 dr -2 u238 dt 3 fl08
det cxs14u238 du -14 de 2 dr -2 u238 dt 3 fl14
det cxs22u238 du -22 de 2 dr -2 u238 dt 3 fl22
det cxs02h1   du -02 de 2 dr -2 h1   dt 3 fl02
det cxs17h1   du -17 de 2 dr -2 h1   dt 3 fl17
det cxs02y89  du -02 de 2 dr -2 y89  dt 3 fl02
det cxs17y89  du -17 de 2 dr -2 y89  dt 3 fl17
% ---Micro Scattering---
det sxs04n14  du -04 de 2 dr -3 n14  dt 3 fl04
det sxs08n14  du -08 de 2 dr -3 n14  dt 3 fl08
det sxs14n14  du -14 de 2 dr -3 n14  dt 3 fl14
det sxs22n14  du -22 de 2 dr -3 n14  dt 3 fl22
det sxs04n15  du -04 de 2 dr -3 n15  dt 3 fl04
det sxs08n15  du -08 de 2 dr -3 n15  dt 3 fl08
det sxs14n15  du -14 de 2 dr -3 n15  dt 3 fl14
det sxs22n15  du -22 de 2 dr -3 n15  dt 3 fl22
det sxs04u235 du -04 de 2 dr -3 u235 dt 3 fl04
det sxs08u235 du -08 de 2 dr -3 u235 dt 3 fl08
det sxs14u235 du -14 de 2 dr -3 u235 dt 3 fl14
det sxs22u235 du -22 de 2 dr -3 u235 dt 3 fl22
det sxs04u238 du -04 de 2 dr -3 u238 dt 3 fl04
det sxs08u238 du -08 de 2 dr -3 u238 dt 3 fl08
det sxs14u238 du -14 de 2 dr -3 u238 dt 3 fl14
det sxs22u238 du -22 de 2 dr -3 u238 dt 3 fl22
det sxs02h1   du -02 de 2 dr -3 h1   dt 3 fl02
det sxs17h1   du -17 de 2 dr -3 h1   dt 3 fl17
```

```
det sxs02y89  du -02 de 2 dr -3 y89  dt 3 fl02
det sxs17y89  du -17 de 2 dr -3 y89  dt 3 fl17
% ---Micro Fission---
det fxs04u235 du -04 de 2 dr -6 u235 dt 3 fl04
det fxs08u235 du -08 de 2 dr -6 u235 dt 3 fl08
det fxs14u235 du -14 de 2 dr -6 u235 dt 3 fl14
det fxs22u235 du -22 de 2 dr -6 u235 dt 3 fl22
det fxs04u238 du -04 de 2 dr -6 u238 dt 3 fl04
det fxs08u238 du -08 de 2 dr -6 u238 dt 3 fl08
det fxs14u238 du -14 de 2 dr -6 u238 dt 3 fl14
det fxs22u238 du -22 de 2 dr -6 u238 dt 3 fl22
% ---Micro Nubar---
det nb04u235 du -04 de 2 dr -7 u235 dt 3 fxs04u235
det nb08u235 du -08 de 2 dr -7 u235 dt 3 fxs08u235
det nb14u235 du -14 de 2 dr -7 u235 dt 3 fxs14u235
det nb22u235 du -22 de 2 dr -7 u235 dt 3 fxs22u235
det nb04u238 du -04 de 2 dr -7 u238 dt 3 fxs04u238
det nb08u238 du -08 de 2 dr -7 u238 dt 3 fxs08u238
det nb14u238 du -14 de 2 dr -7 u238 dt 3 fxs14u238
det nb22u238 du -22 de 2 dr -7 u238 dt 3 fxs22u238
% ---Micro (n, 2n)---
det n2n04n14  du -04 de 2 dr 16 n14  dt 3 fl04
det n2n08n14  du -08 de 2 dr 16 n14  dt 3 fl08
det n2n14n14  du -14 de 2 dr 16 n14  dt 3 fl14
det n2n22n14  du -22 de 2 dr 16 n14  dt 3 fl22
det n2n04n15  du -04 de 2 dr 16 n15  dt 3 fl04
det n2n08n15  du -08 de 2 dr 16 n15  dt 3 fl08
det n2n14n15  du -14 de 2 dr 16 n15  dt 3 fl14
det n2n22n15  du -22 de 2 dr 16 n15  dt 3 fl22
det n2n04u235 du -04 de 2 dr 16 u235 dt 3 fl04
det n2n08u235 du -08 de 2 dr 16 u235 dt 3 fl08
det n2n14u235 du -14 de 2 dr 16 u235 dt 3 fl14
det n2n22u235 du -22 de 2 dr 16 u235 dt 3 fl22
det n2n04u238 du -04 de 2 dr 16 u238 dt 3 fl04
det n2n08u238 du -08 de 2 dr 16 u238 dt 3 fl08
det n2n14u238 du -14 de 2 dr 16 u238 dt 3 fl14
det n2n22u238 du -22 de 2 dr 16 u238 dt 3 fl22
det n2n02y89  du -02 de 2 dr 16 y89  dt 3 fl02
det n2n17y89  du -17 de 2 dr 16 y89  dt 3 fl17
% ---Micro (n, 3n)---
det n3n04u235 du -04 de 2 dr 17 u235 dt 3 fl04
det n3n08u235 du -08 de 2 dr 17 u235 dt 3 fl08
det n3n14u235 du -14 de 2 dr 17 u235 dt 3 fl14
det n3n22u235 du -22 de 2 dr 17 u235 dt 3 fl22
det n3n04u238 du -04 de 2 dr 17 u238 dt 3 fl04
det n3n08u238 du -08 de 2 dr 17 u238 dt 3 fl08
det n3n14u238 du -14 de 2 dr 17 u238 dt 3 fl14
det n3n22u238 du -22 de 2 dr 17 u238 dt 3 fl22
% ---Thermal Scattering Libraries---
thermstoch u 951 u-un.45t u-un.46t
thermstoch n 951 n-un.45t n-un.46t
thermstoch y 964 y-yh2.45t y-yh2.46t
```

```
thermstoch h 964 h-yh2.45t h-yh2.46t
therm be be-met.43t
% ---Materials---
mat monolith -7.9 tmp 937
    6012.02c 0.00190000 14028.02c 0.00926426 14029.02c 0.00047226
   14030.02c 0.00031149 15031.02c 0.00041300 16032.02c 0.00024697
   16033.02c 0.00000195 16034.02c 0.00001105 16036.02c 0.00000003
   24050.02c 0.00790729 24052.02c 0.15248425 24053.02c 0.01729049
   24054.02c 0.00430397 25055.02c 0.01027400 26054.02c 0.03900800
   26056.02c 0.61179900 26057.02c 0.01413640 26058.02c 0.00133360
   28058.02c 0.07747370 28060.02c 0.02984250 28061.02c 0.00129740
   28062.02c 0.00413670 28064.02c 0.00105380 42092.02c 0.00212480
   42094.02c 0.00132920 42095.02c 0.00230180 42096.02c 0.00241780
   42097.02c 0.00138950 42098.02c 0.00352300 42100.02c 0.00141270
mat fuel -14.3 tmp 951 moder u 92238 moder n 7014
   92235.02c 0.1975     92238.02c 0.8025
    7014.02c 0.996       7015.02c 0.004
mat moderator -4.3 tmp 964 moder y 39089 moder h 1001
   39089.02c 1           1001.02c 2
mat htpipe -2.267 tmp 928
   14028.02c 4.11552E-4 14029.02c 2.08976E-5 14030.02c 1.37758E-5
   24050.02c 1.77806E-4 24052.02c 3.42886E-3 24053.02c 3.88795E-4
   24054.02c 9.67787E-5 25055.02c 4.56726E-4 26054.02c 8.58252E-4
   26056.02c 1.34726E-2 26057.02c 3.11151E-4 26058.02c 4.14072E-5
   28058.02c 1.74225E-3 28060.02c 6.71125E-4 28061.02c 2.91727E-5
   28062.02c 9.30147E-5 28064.02c 2.36883E-5 42092.02c 4.83027E-5
   42094.02c 3.01072E-5 42095.02c 5.18174E-5 42096.02c 5.42900E-5
   42097.02c 3.10836E-5 42098.02c 7.85385E-5 42100.02c 3.13435E-5
   11023.02c 4.92833E-3
mat reflector -1.854 tmp 600 moder be 4009
      4009.01c 1
% ---Microscopic Materials---
mat n14  1 tmp 951 moder n  7014  7014.02c 1
mat n15  1 tmp 951                7015.02c 1
mat u235 1 tmp 951               92235.02c 1
mat u238 1 tmp 951 moder u 92238 92238.02c 1
mat y89  1 tmp 964 moder y 39089 39089.02c 1
mat h1   1 tmp 964 moder h  1001  1001.02c 1
```

APPENDIX C. SELECTED MICROSCOPIC CROSS SECTIONS

This appendix contains thermal microscopic cross section data for selected isotopes and regions in the 2D single assembly configuration. The following data are included as an appendix for a complete description of the benchmark problem against which multigroup data of other benchmark problems are compared, but not within the text as the effect of core environment discussed in CHAPTER 4 perturbs the microscopic cross sections in a similar fashion to the macroscopic cross sections.

C.1 Fast Data

Table 41 contains fast group microscopic data for the four composing isotopes (^{14}N, ^{15}N, ^{235}U, and ^{238}U) in fuel pins #4, #8, #14 and #22 for the 2D single assembly case.

Table 41 – Microscopic Data for Fuel in 2D Assembly Configuration, Group 1 of 2

Isotope	Data (% 1σ)	Pin 04	Pin 08	Pin 14	Pin 22
^{14}N	Total σ (b)	4.584 (0.01)	4.589 (0.01)	4.587 (0.01)	4.358 (0.01)
	Capture σ (b)	0.06147 (0.01)	0.06025 (0.01)	0.05817 (0.01)	0.05375 (0.01)
	Scatter σ (b)	4.519 (0.01)	4.526 (0.01)	4.527 (0.01)	4.302 (0.01)
^{15}N	Total σ (b)	3.432 (0.01)	3.439 (0.01)	3.450 (0.01)	3.435 (0.01)
	Scatter σ (b)	3.429 (0.01)	3.436 (0.01)	3.447 (0.01)	3.433 (0.01)
^{235}U	Total σ (b)	15.89 (0.01)	15.81 (0.01)	15.64 (0.01)	14.30 (0.01)
	Capture σ (b)	2.144 (0.01)	2.114 (0.01)	2.054 (0.01)	1.638 (0.02)
	Scatter σ (b)	7.597 (0.01)	7.618 (0.01)	7.645 (0.01)	7.504 (0.01)
	Fission σ (b)	5.135 (0.01)	5.069 (0.01)	4.942 (0.01)	4.128 (0.01)
	Nubar	2.513 (0.01)	2.511 (0.01)	2.509 (0.01)	2.507 (0.01)
^{238}U	Total σ (b)	10.62 (0.01)	10.64 (0.01)	10.66 (0.01)	10.47 (0.01)
	Capture σ (b)	0.5440 (0.02)	0.5401 (0.02)	0.5321 (0.02)	0.4486 (0.02)
	Scatter σ (b)	8.572 (0.01)	8.608 (0.01)	8.660 (0.01)	8.525 (0.01)
	Fission σ (b)	0.1040 (0.01)	0.1017 (0.01)	0.0978 (0.02)	0.0921 (0.02)
	Nubar	2.564 (0.01)	2.563 (0.01)	2.560 (0.01)	2.559 (0.01)

Table 42 contains fast group microscopic data for the two composing isotopes (^{1}H and ^{89}Y) in moderator rods #2 and #17 for the 2D single assembly case.

Table 42 – Microscopic Data for Moderator in 2D Assembly Configuration, Group 1 of 2

Isotope	Data (% 1σ)	Rod 02	Rod 17
^{1}H	Total σ (b)	12.35 (0.01)	12.04 (0.01)
	Capture σ (b)	0.004045 (0.01)	0.003240 (0.01)
	Scatter σ (b)	12.34 (0.01)	12.03 (0.01)
^{89}Y	Total σ (b)	6.642 (0.01)	6.681 (0.01)
	Capture σ (b)	0.02418 (0.02)	0.02175 (0.02)
	Scatter σ (b)	6.452 (0.01)	6.505 (0.01)

C.2 Thermal Data

Table 43 contains thermal group microscopic data for the four composing isotopes (^{14}N, ^{15}N, ^{235}U, and ^{238}U) in fuel pins #4, #8, #14 and #22 for the 2D single assembly case.

Table 43 – Microscopic Data for Fuel in 2D Assembly Configuration, Group 2 of 2

Isotope	Data	Pin 04		Pin 08		Pin 14		Pin 22	
^{14}N	Total σ (b)	8.888	(0.02)	8.898	(0.02)	8.906	(0.02)	8.975	(0.03)
	Capture σ (b)	0.6937	(0.02)	0.6905	(0.02)	0.6883	(0.02)	0.6664	(0.03)
	Scatter σ (b)	8.195	(0.02)	8.208	(0.02)	8.218	(0.02)	8.309	(0.03)
^{15}N	Total σ (b)	4.455	(0.02)	4.454	(0.02)	4.454	(0.02)	4.448	(0.03)
	Scatter σ (b)	4.455	(0.02)	4.454	(0.02)	4.454	(0.02)	4.448	(0.03)
^{235}U	Total σ (b)	237.7	(0.02)	236.3	(0.02)	235.4	(0.02)	226.6	(0.03)
	Capture σ (b)	35.77	(0.02)	35.55	(0.02)	35.39	(0.02)	34.00	(0.03)
	Scatter σ (b)	13.59	(0.02)	13.58	(0.02)	13.58	(0.02)	13.56	(0.03)
	Fission σ (b)	188.3	(0.02)	187.2	(0.02)	186.4	(0.02)	179.1	(0.03)
	Nubar	2.432	(0.02)	2.432	(0.02)	2.432	(0.02)	2.432	(0.03)
^{238}U	Total σ (b)	12.03	(0.02)	12.01	(0.02)	12.00	(0.02)	11.87	(0.03)
	Capture σ (b)	1.003	(0.02)	0.9985	(0.02)	0.9955	(0.02)	0.9656	(0.03)
	Scatter σ (b)	11.02	(0.02)	11.01	(0.02)	11.00	(0.02)	10.91	(0.03)
	Nubar	2.443	(0.02)	2.443	(0.02)	2.443	(0.02)	2.443	(0.03)

Table 44 contains thermal group microscopic data for the two composing isotopes (^{1}H and ^{89}Y) in moderator rods #2 and #17 for the 2D single assembly case.

Table 44 – Microscopic Data for Moderator in 2D Assembly Configuration, Group 2 of 2

Isotope	Data	Rod 02		Rod 17	
^{1}H	Total σ (b)	30.68	(0.01)	30.45	(0.02)
	Capture σ (b)	0.01493	(0.02)	0.1472	(0.02)
	Scatter σ (b)	30.53	(0.01)	30.30	(0.02)
^{89}Y	Total σ (b)	8.269	(0.01)	8.260	(0.02)
	Capture σ (b)	0.5732	(0.02)	0.5652	(0.02)
	Scatter σ (b)	7.695	(0.01)	7.695	(0.02)

REFERENCES

[1] M. D. DEHART, J. ORTENSI, and V. M. LABOURÉ, "NEAMS FY20 Assessment Problem Draft," INL/MIS-21-62472, Rev. 0, Idaho National Laboratory (June 2020).

[2] C. MATTHEWS, R. B. WILKERSON, R. C. JOHNS, H. R. TRELLUE, and R. C. MARTINEAU, "Task 1: Evaluation of M&S tools for micro-reactor concepts," LA-UR-19-22263, Los Alamos National Laboratory (April 2019).

[3] C. MATTHEWS et al., "Coupled Multiphysics Simulations of Heat Pipe Microreactors Using DireWolf," Nuclear Technology, **207**, *7*, 1142 (2021); https://doi.org/10.1080/00295450.2021.1906474.

[4] J. LEPPÄNEN, M. PUSA, T. VIITANEN, V. VALTAVIRTA, and T. KALTIAISENAHO. "The Serpent Monte Carlo code: Status, development and applications in 2013." Ann. Nucl. Energy, **82**, 142 (2015); https://doi.org/10.1016/j.anucene.2014.08.024.

[5] F. RAHNEMA. "Boundary Condition Perturbation Theory for Use in Spatial Homogenization Methods," Nuclear Science and Engineering, **102**, *2*, 183 (1989); https://doi.org/10.13182/NSE89-3.

[6] J.L. CONLIN, W. HAECK, D. NEUDECKER, D.K. PARSONS, and M.C. WHITE. "Release of ENDF/B-VIII.0-Based ACE Data Files," LA-UR-18-24034, Los Alamos National Laboratory (May 2018).

[7] D.K. PARSONS and C.A. TOCCOLI. "Re-Release of the ENDF/B VIII.0 $S(\alpha,\beta)$ Data Processed by NJOY2016," LA-UR-20-24456, Los Alamos National Laboratory (June 2020).